Knee function through Finite Element Analysis and the role of Miocene hominoids to understand the origin of antipronograde behaviours: the *Pierolapithecus catalaunicus*' patella as a test-case study

MARTA PINA[1,2,*], DANIEL DeMIGUEL[3,4,1], FRANCESC PUIGVERT[5], JORDI MARCÉ-NOGUÉ[6,5,1] and SALVADOR MOYÀ-SOLÀ[1,7,8]

[1]Institut Català de Paleontologia Miquel Crusafont, Universitat Autònoma de Barcelona, Edifici ICTA-ICP, c/ Columnes s/n, Campus de la UAB, 08193 Cerdanyola del Vallès, Barcelona, Spain; e-mail: salvador.moya@icp.cat

[2]*Current address:* Department of Zoology, Graduate School of Science, Kyoto University, Kitashirakawa Oiwake-cho, Sakyo-ku, Kyoto 606-8502, Japan; e-mail: pina@anthro.zool.kyoto-u.ac.jp

[3]Fundación ARAID, Zaragoza, Spain

[4]Departamento de Ciencias de la Tierra, Área de Paleontología. Universidad de Zaragoza, c/ Pedro Cerbuna, 12, 50009, Zaragoza, Spain; e-mail: demiguel@unizar.es

[5]Departament de Resistència de Materials i Estructures a l'Enginyeria, Universitat Politècnica de Catalunya, BarcelonaTech, Colom 11, 08222, Terrassa, Spain; e-mail: fpuigvert@gmail.com

[6]Centrüm für Naturkunde, University of Hamburg, Martin-Luther-King-Platz 3, 20146, Hamburg, Germany; e-mail: Jordi.marce.nogue@uni-hamburg.de

[7]Institució Catalana de Recerca i Estudis Avançats (ICREA), Pg. Lluís Companys 23, 08010, Barcelona, Spain.

[8]Unitat d'Antropologia Biològica, Departament de Biologia Animal, Biologia Vegetal i Ecologia, Universitat Autònoma de Barcelona, 08193 Cerdanyola del Vallès, Barcelona, Spain.

* Corresponding author

Abstract: Although extensive research has been carried out in recent years on human bipedalism origin and evolution, a full understanding of this question is far to be achieved. In this regard, the role of Miocene hominoids emerges as key to better comprehend the locomotor types observed in living apes and humans. *Pierolapithecus catalaunicus*, an extinct stem great ape from the middle Miocene (c. 12.0 Ma) of the Vallès-Penedès Basin (NE Iberian Peninsula), is the first undoubted hominoid with an orthograde (erected) body plan. Its locomotor repertoire included above-branch quadrupedalism and other antipronograde behaviours. Elucidating the adaptive features present in the *Pierolapithecus* skeleton and its associated biomechanics helps us to better understand the origin of hominoid orthogrady. This work represents a new biomechanical perspective on the *Pierolapithecus* locomotion, by studying its patella among a large sample of extant anthropoids. This is the first time that the biomechanical patellar performance in living non-human anthropoids and a stem hominid is studied through Finite Element Analysis (FEA). Differences in stress distribution are found depending on body plan and the presence/absence of a distal apex, probably due to dissimilar biomechanical performances. *Pierolapithecus*' biomechanical response mainly resembles that of great apes, suggesting a similar knee joint use in mechanical terms. These results underpin previous studies on *Pierolapithecus*, favouring the idea that a relevant degree of some antipronograde behaviour may have made up part of its locomotor repertoire. Moreover, our results corroborate the presence of modern great ape-like knee biomechanical performances back in the Miocene.

Key words: knee, patellar biomechanics, *Pierolapithecus catalaunicus*, antipronograde behaviours evolution, Miocene.

Pierolapithecus catalaunicus is an extinct primate from the middle Miocene (late Aragonian, c. 12.0 Ma) found in the Barranc de Can Vila 1 locality (within the Abocador de Can Mata Series, Els Hostalets de Pierola) in the Vallès-Penedès Basin (NE Iberian Peninsula; Moyà-Solà *et al.* 2004; Casanovas-Vilar *et al.* 2011; Alba *et al.* 2017). Moyà-Solà and colleagues (2004) identified this taxon as a stem hominid (early member of the great apes and human clade). Some years later, these authors suggested that *Pierolapithecus* could be placed closer to the pongines, based on the internal morphology of its splachnocranium (Pérez de los Ríos *et al.* 2012; see also Alba 2012). On the other hand, Begun & Ward (2005) and Begun (2009, 2015) proposed that *Pierolapithecus* might be a stem hominin. Despite its phylogenetic affinities remaining controversial, *Pierolapithecus* undoubtedly belong to the subfamily Dryopithecinae (Casanovas-Vilar *et al.* 2011; Alba 2012; Pérez de los Ríos *et al.* 2012).

The discovery of more than 80 elements belonging to a single individual of *Pierolapithecus*, including both cranial and postcranial elements, allows us to reconstruct its body plan and positional behaviour (Moyà-Solà *et al.* 2004). The rib curvature, a long clavicle, and the lumbar vertebral morphology (neural process caudally oriented and transverse processes inserted in the pedicle-body junction, among other traits) suggest that *Pierolapithecus* might exhibit an orthograde body plan with a broad and shallow thorax (Moyà-Solà *et al.* 2004; Susanna *et al.* 2010*a, b*). The shape of the metacarpals and phalanges is mostly primitive (short, proximodorsally tilted, flat, and wide proximal articular facet, and large and widely separated plantar tubercles surrounding a deep central depression) and suggests powerful-grasping palmigrady (Moyà-Solà *et al.* 2004, 2005; Almécija *et al.* 2009). These palmigrady-related features are symplesiomorphies shared with other early Miocene apes, such as *Ekembo*, and are commonly associated with the tail loss and aiding with balance to avoid toppling from

branches (Cartmill 1985; Kelley 1997; Almécija *et al.* 2009). In addition, phalanges are not markedly curved as in suspensory primates (Moyà-Solà *et al.* 2004, 2005; Almécija *et al.* 2009; Alba *et al.* 2010). However, Deane & Begun (2008, 2010) argued that *Pierolapithecus* could exhibit a significant degree of suspensory behaviours, based on its phalangeal curvature. Afterwards, Alba *et al.* (2010) provided additional data against the hypothesis of these authors (Deane & Begun 2008, 2010), but it is important to be cautious about sharply refusing the presence of suspensory habits in this taxon when the evidence is based exclusively on a single anatomical element.

Other anatomical regions, such as the pelvis and the knee, show a mixture of primitive features (e.g., deep concave gluteal surface and isthmus form at the ilium, caudal acetabulum and linea arcuate form, sacroiliac joint morphology, and pubis position) and incipient orthograde-like affinities (flared ilium, width of the iliac tuberosity, mediolaterally wide and anteroposterior thin patella; Hammond *et al.* 2013; Pina *et al.* 2014*a*). Moreover, the wrist displays an important synapomorphy among hominids, the lack of contact between the ulna and the triquetrum, which has been associated with vertical climbing behaviours (Moyà-Solà *et al.* 2004).

Thus, *Pierolapithecus* shows some primitive features (e.g., slightly curved phalanges, with a short, flat, and wide proximal articular facets, large and separated plantar tubercles, a deep central depression, and an iliac concave gluteal surface) combined with derived traits (e.g., rib curvature, long clavicle, caudally oriented neural vertebral processes, transverse vertebral processes inserted in the pedicle-body junction, lack of contact ulna-triquetrum, flared ilium, and great ape-like patellar shape), which altogether suggest that above-branch quadrupedalism still remained an important component of its locomotor behaviour. This taxon would have combined this type of locomotion with other novel antipronograde positional behaviours, a mixture which is

currently unseen in living hominoids but that was common in the Miocene taxa (Rose 1983; Moyà-Solà *et al.* 2004; Almécija *et al.* 2009; Pina *et al.* 2014*a*). Therefore, *Pierolapithecus* most likely would have displayed some degree of modern ape-like behaviours, such as vertical climbing (Moyà-Solà *et al.* 2004; Almécija *et al.* 2009). Although the important role of the forelimb in hominoid locomotion is undeniable (Larson 1998; Hunt 2016), the hind limb also takes an active role in orthograde locomotor modes (Preuschoft 1970, 2004; Badoux 1974; Crompton *et al.* 2010), most noticeable in the case of terrestrial bipedalism (Lovejoy 2005, 2007; Crompton *et al.* 2010). In addition, the middle Miocene is a key "starting-point" for the antipronograde (orthograde-like) behaviours shown nowadays in the apes-and-humans clade, since we find at this moment the first unquestionable orthograde hominoids, such as *Pierolapithecus*. Therefore, the study of the Miocene hominoids hind limb is essential to better understand locomotor evolution within the Hominoidea, including human bipedalism. In this regard, the only complete non-pedal hind limb element preserved for *Pierolapithecus* is a left patella (Pina *et al.* 2014*a*, fig. 1). Its general morphology clearly resembles those of great apes, by being relatively broad mediolaterally, short proximodistally, and thin anteroposteriorly (Pina *et al.* 2014*a*). In contrast, the patellar external morphology of *Pierolapithecus* departs from that of monkeys, the latter displaying a relatively narrower mediolateral, longer proximodistal, and thicker anteroposterior patellae (Pina *et al.* 2014*a*). As the patellar shape has been traditionally associated with the functionality of the knee (Ward *et al.* 1995), a versatile joint with a high range of movements was inferred for *Pierolapithecus* based on shape similarities with great apes (Pina *et al.* 2014*a*). Given that antipronograde suspensory behaviors are unlikely for *Pierolapithecus* on the basis of other anatomical regions (see above), it was proposed that this versatility was related to vertical climbing (Pina *et al.* 2014*a*).

Moreover, Pina *et al.* (2014*a*) noticed that the patella of *Pierolapithecus* would differ from that of earlier hominoids, which probably show the plesiomorphic condition (with a slightly anteroposteriorly thinner patella than living great apes; Ward *et al.* 1995). Thus, the patella of *Pierolapithecus* might represent a more derived stage in the hominoid patellar shape evolution and its biomechanical study could be highly useful for a better comprehension of the function and biomechanics of the hominoid knee from an evolutionary perspective.

Although the postcranial morphology of the Vallès-Penedès hominoids has been extensively studied (Moyà-Solà & Köhler 1996; Moyà-Solà *et al.* 2004; Almécija *et al.* 2009; Alba *et al.* 2015; among others), analyses of their postcranium using quantitative biomechanical approaches are scarce (Pina *et al.* 2012, 2014b; Pina 2016). Moreover, the incompleteness of the unearthed fossils and/or the lack of an anatomical context (e.g., only one element of the knee has been found for this joint in *Pierolapithecus*) make new techniques such as Finite Element Analysis (FEA) essential to address biomechanical questions in extinct taxa. FEA allows us to investigate the biomechanical response (how stress is distributed under specific loads) in an isolated bone (patella) within a broad anatomical context (knee joint), given that no other element of the knee is available for this taxon. Additionally, we can digitally manipulate the original geometries (adding and/or removing structures, changing the magnitude of specific traits, etc.) to better comprehend one of the most enduring questions in palaeontology, the relationship between bone shape and function. Given that all the patellae are treated under the same model based on human kinematics (see next section), we seek here to directly test how different anthropoid patellar shapes influence biomechanical response to a human-like dynamic movement (knee flexion) and examine whether the *Pierolapithecus* patella responses similarly than those of great apes, as previously

suggested by its morphology (Pina *et al. 2014a*). We also investigate the role of the distal apex (i.e., patellar shape) on a human-like locomotor performance in a comparative sample of living anthropoids. This is the first attempt to analyse the patella of a Miocene hominoid within a large sample of extant anthropoid primates using FEA, as well as the first work in which non-human anthropoid (NHA) patellae are tested through this methodology.

MATERIAL AND METHODS

Sample of study

The main object of study is the patella (IPS 21350.37) of the stem hominid *Pierolapithecus catalaunicus* (Moyà-Solà *et al.* 2004; Pina *et al.* 2014*a*). IPS21350.37 is the only complete (non-pedal) hind limb element within the *Pierolapithecus* skeleton (Moyà-Solà *et al.* 2004; Pina *et al.* 2014*a*). This specimen is housed at the Institut Català de Paleontologia Miquel Crusafont (ICP, Spain).

The comparative sample consists of 11 different patellar three-dimensional (3D) models of living anthropoid species (Pina *et al.* 2019, appendix S1; Table 1). The original patellae are housed at the American Museum of Natural History (AMNH; New York, US), the Museum of Comparative Zoology – Harvard University (MCZ; Cambridge, US), and Stony Brook University (SBU; Stony Brook, US; Table 1). These bones were scanned between 2012 and 2015 by using either a surface laser scanner (NextEngine) or a computed tomography (CT) scanner (see parameters of the final geometries in Table 1). This is the first time that a wide sample of NHA patellae is analysed through FEA. The sample comprises all major taxonomic groups of anthropoids, including platyrrhines (*Cebus* and *Ateles*), cercopithecines (*Cercopithecus* and *Mandrillus*), colobines (*Colobus*), lesser apes (*Hylobates* and *Symphalangus*), Asian (*Pongo*) and

African (*Pan* and *Gorilla*) great apes, and modern humans (*Homo*). Moreover, this sample represents the high variety of locomotor modes performed by living anthropoids. Monkeys (*Cebus*, cercopithecines and colobines) are pronograde quadrupedal primates, either arboreal (*Cebus*, *Colobus*, and *Cercopithecus*) or terrestrial (*Mandrillus*; McGraw 1996, 1998; Fleagle 2013). Quadrupedalism is characterized by the progression along approximately horizontal supports by using the four limbs, which contact these supports in a particular sequence (Hunt *et al.* 1996). African great apes are knuckle-walkers, a type of quadrupedalism performed by lying the dorsal face of the second phalanges of the hand on the ground (Hunt *et al.* 1996). The sample also incorporates suspensory primates, those that progress through an arboreal setting by hanging below the supports (Hunt *et al.* 1996). The most common example of suspensory primates are orangutans (Sugardjito 1982), however, other types of suspension are also included in this category: atelids (*Ateles*) tail-assisted suspension with the participation of their prehensile tail (Youlatos 2002); and hylobatids brachiation (*Hylobates* and *Symphalangus*) that incorporates aerial phases during displacement (Fleagle 1976). Finally, humans are terrestrial bipeds (Senut 2016), locomoting along a continuous, horizontal or oblique support by only using the hind limbs (Hunt 1992; Fleagle 2013).

Knee modelling

FEA (Rayfield 2007; Bright 2014) is used here to inspect the patellar response to knee flexion in a group of living and fossil primates, as well as to assess the effect of morphological changes in several models. Given that the NHA patellar kinematics are still largely unknown, the human knee is taken as reference to construct the models. The patella makes up part of a complicated and sophisticated system, which remains

controversial even for the highly studied human knee. The human patella is embedded within the ligaments and muscles of the quadriceps complex and the synovial capsule of the knee joint (see a schematic representation in Platzer 2008). The patella develops within the quadriceps tendon and some authors suggest that the quadriceps expands and passes along the posterior side of the patella to join the patellar tendon under the superficial fibres of the latter. In contrast, other authors advocate for differentiation of the quadriceps tendon into separate tendons, quadriceps and patellar (see a detailed summary in Samuels *et al.* 2017 and references therein). Since resolving anatomical knee issues is outside the scope of our study and this discussion does not directly affect our models, we consider the quadriceps and the patellar tendons as separate units to clearly limit the constraint areas of the model (see next subsection). The forces in the patello-femoral joint are a function of the quadriceps muscle force, and the angle of flexion of the knee (Nisell 1985; Schindler & Scott 2011). The most superficial parts of the patella are in tension due to the action of two opposite forces, that of the quadriceps muscle and that of the patellar tendon (Oxnard 1971 fig. 1 for a diagram of forces acting in a semi-flexed knee). The contact between the femur and the patella displaces proximally during knee flexion and generates a patellar reaction force (F), which increases progressively during this movement (Nisell 1985; Lovejoy 2007; Masouros *et al.* 2010).

The most important issues for generating a rigorous knee model relate to the inherent complexity of this joint, the number of elements, and the six degrees of freedom between the femur and the tibia (see above; Heegaard *et al.* 1995; Masouros *et al.* 2010; Samuels *et al.* 2017). In order to create an easy-to-analyse, realistic and comparable model, the human knee joint was simplified in our modelling approach. Specifically, only the solid elements (bones) and basic forces acting in the patella during flexion

were modelled (Fig. 1). This model results in two forces that stretch the patella in opposite directions due to the action of the quadriceps muscle (QM) and the patellar tendon (PT), and a third force (F) resulting from the contact between the patellar articular surface and the patellar groove at the distal femur (Fig. 1). The direction of F also changes with the flexion of the knee, being almost perpendicular to the main anteroposterior axis of the patella and becoming more vertical (related to the horizontal line) in a flexed position (Fig. 1). Lateral movement of the patella during flexion (Q angle) has not been included in this work since no angle data are available for the selected NHA sample and we intend to model a comparable scenario for all the included taxa.

Model construction

Patellar 3D models were obtained from both superficial laser or CT scanning. In the latter case, density thresholding was selected following variations in the grey scale (bone densities) by checking changes in Hounsfield units (Hounsfield 1973, 1976; Ohman *et al.* 1997). Once the bone was isolated, only the external surface was selected for FEA. Models were imported to the software Rhinoceros 5.0 to repair and refine the surface meshes. Given that the inner structure of the *Pierolapithecus* patella is highly mineralized, CT scanning results were not satisfactory, displaying broad areas of brightness that did not allow the visualization of the trabecular tissue (M.P. pers. obs.). Therefore, as *Pierolapithecus* is the main subject of this study, we considered the patella of all taxa as solid objects. Although Cazenave *et al.* (2019) showed that the proportion of trabecular/cortical bone in the patellae of chimpanzees and humans is different, other studies support our assumption of modelling bones as solid objects. These studies highlight the fact that the simplification of trabecular tissue for FEA has implications on

stress magnitudes (Toro-Ibacache *et al.* 2016; Godinho *et al.* 2017) and just in localized areas (Fitton *et al.* 2015) of the model, but not in the general deformation of the model (Fitton *et al.* 2015; Toro-Ibacache *et al.* 2016; Godinho *et al.* 2017). Given that our work is purely comparative, the absolute stress values (magnitude) do not affect our results on stress distribution (as occurs in the case of the material properties; see next subsection). Additionally, Gröning *et al.* (2013) suggested that mechanical adaptations can be tested in models with a hypothetical internal structure, including solid models with no internal cavities, producing reliable results when general patterns of deformation are tested (see also Fitton *et al.* 2015).

Thus, the obtained polygonal models were converted to solid CAD (computer-aided design) objects using engineering techniques (Marcé-Nogué *et al.* 2011). Irregularities in the CAD models using tools in Rhinoceros 5.0. Final FE models were meshed with an adaptive mesh of 10-noded tetrahedral elements (Marcé-Nogué *et al.* 2015) to create a model of an appropriate level of accuracy and density to capture the stress patterns and variations, and assure the reliability of results (Dumont *et al.* 2009; Tseng & Flynn 2014). Table 1 reports final geometric properties of the 15 3D patellar models.

Material properties

Isotropic, homogeneous and linear elastic properties were assumed for the models. Mechanical properties of the human patella cortical bone were applied following Heegaard *et al.* (1995): Young's modulus E = 15 GPa, and Poisson ratio $\nu = 0.3$. It must be stressed, however, that these values are not crucial for this study due to its comparative nature, since the equations of elasticity used in FEA for linear isotropic and homogeneous materials do not affect stress patterns (DeMiguel *et al.* 2015; Gil *et al.* 2015).

Constraints and loading conditions

As above-mentioned, the anatomy of the patella is still controversial including the degree of differentiation of the quadriceps tendon into quadriceps and patellar tendons (Samuels *et al.* 2017). However, in order to virtually implement the knee kinematic model, we selected two areas of attachment (constrained regions) to fix the models, those of the QM and the PT (Fig. 2A). These areas were selected by following the boundaries of the most rugose area at the posterior and proximal side of the patellar body for the QM; and the posterior area of the apex for the PT. In the case of the apex-less patellae, the selected PT region comprised the posterior region of the bone expanding from its most distal point, to the distal edge of the patellar surface. Thus, this reconstruction generates an extrinsic approach where the forces will be generated by the reaction at the constraints. Previous work proposed such an extrinsic approach as a way to study the mechanical behaviour of bony structures (e.g., Preuschoft & Witzel 2002). This approach allows us to change the position and direction of the contact force F to generate the different scenarios proposed.

The articular surface of the patella was divided in three strips to simulate the proximal displacement of the patello-femoral contact during knee flexion (Fig. 2B; Schindler & Scott 2011), from extended (distal strip), to semi-flexed (central strip), and fully-flexed (proximal strip). In each of the steps (i.e., every strip) a pressure (F) was applied with an increased angle related to the anteroposterior horizontal line (see a model in Schindler & Scott 2011). Given that the scope of our work is purely comparative, the absolute values of this angle are not relevant. Thus, the F angle was thus implemented as follows to emphasize differences among the patellae of the sample: 0º (extended knee–initial

position of the knee), 30º (semi-flexed knee–intermediate value), and 60º (full-flexed knee–magnified angle value; Fig. 2B).

Scaling forces

Patellae 3D models included in this study are very diverse in size, ranging from the smallest *Cebus olivaceus* (mean body mass ~3 kg; Smith & Jungers 1997) to *Gorilla gorilla* (mean body mass ~121 kg, although males can reach more than 170 kg; Smith & Jungers 1997). Therefore, the forces applied to the different patellae were scaled (as originally proposed by Dumont *et al.* 2009) to avoid the size effect of the structure on the results and focus exclusively on the patellar shape role during knee flexion. Scaled forces were calculated by adapting the formulations proposed by Marcé-Nogué *et al.* (2013) to 3D models and following Fortuny *et al.* (2015) to make the patellar models comparable. Equation (1) shows the formula used to calculate the scaled forces applied to the models to obtain von Mises stress values. The patella of *Cercopithecus* was taken as the reference model, with an arbitrary force value of 1 N. Thereby, F_B and V_B are the force and volume of the reference model, respectively; and F_A and V_A the force and volume of the scaled model. Scaled values for the 15 patellae models are listed in Table 2.

$$(1) \qquad F_A = \left(\sqrt[3]{\frac{V_A}{V_B}}\right)^2 F_B$$

As abovementioned, our approach is purely comparative (it compares relative stress values) and is not intended to predict absolute values. Therefore, in vivo or in vitro force values or validation of results against experimental data are not considered necessary for obtaining meaningful results (see e.g., Dumont *et al.* 2005; McHenry *et al.* 2006; Rayfield 2007; DeMiguel *et al.* 2015; Serrano-Fochs *et al.* 2015; Sharp 2015;

Fortuny *et al.* 2016). Hence, scaling forces allow us to analyse the geometries under equivalent loads only taking into account the patellar shape.

FE analyses and results

A structural static analysis was performed for the 15 patellar models using ANSYS 15.0 FE package. In order to compare the models, contour plots of von Mises stress distribution were obtained. This type of stress was selected since it directly measures how the state of stress at any point distorts the material and consequently it is an adequate criterion for predicting the yield of ductile materials when isotropic material properties are used in the organic bone (Doblaré *et al.* 2004; Dumont *et al.* 2009). To aid visualization and comparison of results, a sagittal slice at the mediolateral midpoint of the 15 patellae models was selected (Fig. 2C).

Stress value comparisons

In order to quantify differences among patellae, five biologically homologous points (A to E; Fig. 3) were selected at the mid-sagittal slice of the patellar models. To make them comparable, and considering the great differences in patellar shape, we took the A-E points at the maximum proximodistal height (pr-d) and anteroposterior thickness (a-p) axes of the patellae, where major stress differences were shown. Taking into account the Principle of Saint-Venant (stress can be altered in those areas which are close to the constrains; Dumont *et al.* 2009; Serrano-Fochs *et al.* 2015), points were selected at the 20% and 80% of length from the most proximal point of the pr-d axis (points A and D, respectively); at the 80% of length from the anterior side of the a-p axis (point E); at the intersection between the pr-d and a-p axes (point B); and at the intersection between pr-d and the horizontal line crossing the base of the articular surface (point C; Fig. 3).

Von Mises stress values at these points were recorded at every stage of knee flexion: extended, semi-flexed, and fully-flexed (referred to in the text as 0, 30, and 60, respectively); and they were statistically analysed for the sample of extant anthropoids (Pina *et al.* 2019, appendix S2). The categories considered for testing differences among patellae included presence-absence of apex (with apex *vs* apex-less patellae; Ap), types of body plan (orthograde *vs* pronograde; BP), and the combination of the two previous categories (i.e., pronograde-with apex, orthograde-with apex, and orthograde-without apex; BPAp). Therefore, we evaluated possible differences among groups according to Ap, BP, and BPAp in every stage of knee flexion (0, 30, and 60). Given that the aim of these analyses is to check for differences among groups with known features (e.g., pronogrady-orthogrady), the fossil specimen was not included. Normality of Ap, BP and BPAp was checked through the Shapiro-Wilk test and, afterwards, these variables were analysed through MANOVA and individual ANOVA for each variable. Subsequent group post-hoc comparisons where conducted through the Tukey test. Finally, Principal Component Analysis (PCA) at each knee stage were performed to check major patterns in the data using the variance-covariance matrix. In this case, the patella of *Pierolapithecus* was included in the analysis. Analyses were conducted using the R statistical package (R Core Team 2017).

Experimental FE analyses

In order to inspect the biomechanical role of patellar shape during knee flexion in *Pierolapithecus* and the sample of extant anthropoids, some morphological changes were virtually applied to specific models. Thus, the patellar apex was digitally removed or added in three of the original cases (Pina *et al.* 2019, appendix S1). Firstly, it was removed in the pronograde quadruped *Cercopithecus* (named as *Cercopithecus*-

NoApex), thus allowing to check the biomechanical response of a patella without an apex in a taxon with preferential movements of the hind limb in the parasagittal plane and emphasis on flexion-extension of the knee joint. In these patellae, the distal apex was considered at the base of the articular surface, just where the bone makes an inflection towards the mediolateral centre of the bone. Secondly, the apex was virtually added in the orthograde great apes *Gorilla* (*Gorilla*-WApex) and *Pongo* (*Pongo*-WApex), in order to inspect whether the apex modifies the biomechanical response of the patella during dynamic loading of the joint in two taxa that show a wider range of knee motion, but differential locomotor affinities (since gorillas are orthograde primates that preferentially use the hind limb in compression through knuckle-walking behaviours, whereas orangutans are specialized orthograde suspensors and clambers that use the hind limb mainly in tension; Stern 1975; Crompton *et al.* 2010). In these two cases, the apex was obtained from the *Cercopithecus* patella and consistently fixed to the new one after removing the most distal region of their bone (as explained above, by the point where the bone makes an inflection towards the mediolateral centre). The apex volume was increased proportionally to fit the same proportional length as in the *Cercopithecus* patella.

These modified models generate a final geometry which is not represented in the real world, therefore, its shape cannot be compared and checked with any living species. Due to this problem and the possible intraspecific variability within a taxon, we additionally modified the apex in *Gorilla*-WApex by slightly varying its new apex's volume (15% bigger and smaller), length (one third longer and shorter), inclination related to the anteroposterior axis of the bone (15º more anteriorly and more posteriorly inclined), and shape (more acute and more rounded at the most distal pick; Pina *et al.* 2019, appendices S3, S4). Carrying out these extra analyses allowed us to check if small

differences affect stress distribution in the new modified patellae. As differences were not found (see Pina *et al.* 2019, appendices S3-S5), this additional validation allowed us to use the *Gorilla*-WApex, *Pongo*-WApex, and *Cercopithecus*-NoApex models to make biomechanical inferences related to the patellar shape.

RESULTS

Overall, our results show that von Mises stress values increase from an extended posture of the knee (i.e., forces applied perpendicular to the patellar proximodistal axis) to complete flexion (force tilted 60º relative to the horizontal) in all patellae studied (Fig. 4). Nonetheless, we found differences in patterns of stress distribution in relation to whether patellae belong to orthograde or pronograde primates. All patellae with an apex (i.e., those of platyrrhines, cercopithecoids, hylobatids and humans; Fig. 4A-G, K) display a similar pattern of stress distribution, which follows the direction of the applied force. That is, the highest stress values increasingly separate from the horizontal line anteroposteriorly when the knee is fully flexed. Despite these general similarities, the distribution of von Mises stress differs between pronograde (anthropoid monkeys; Fig. 4A-E) and orthograde (hylobatids and humans; Fig. 4F, G, K) taxa with a patellar apex. Loading produces low stresses (0 to 0.014 MPa) in the distal half of the apex in all pronograde taxa (i.e., *Cebus*, *Ateles*, *Cercopithecus*, *Mandrillus*, and *Colobus*; Fig. 4A-E) during the three phases of flexion, which is particularly evident in *Cercopithecus* and *Colobus* (in which the most distal area remains even free of stress, 0 MPa; Fig. 4C, E). In contrast, the distal apex of orthograde taxa (*Symphalangus* and *Homo*; Fig. 4G, K) experiences higher stress (up to 0.026 MPa) during loading (except in the case of *Hylobates*; Fig. 4F). Figure 4 also illustrates that maximum von Mises stresses is found in the posterior side of the patella in pronograde taxa (0.026 MPa), from the proximal

end to part of the distal half of the bone (in both semi- and full-flexed positions of the knee). High stress is more widely spread (mainly anteroposteriorly) through the whole patella of hylobatids and humans, though it is particularly concentrated in the anterodistal side of the distal half and in the posteroproximal corner of the proximal half (0.002 to 0.026 MPa) in semi-flexed and fully-flexed positions of the knee joint. Surprisingly, the patella of *Hylobates* is almost free of stress during the extended knee phase (showing a maximum stress of 0.006 MPa), where it approximates the pattern found in pronograde taxa for the fully-flexed position (as high stress values are found along the posterior side of the patella and are relatively low at the most distal half apex, 0.014 MPa; Fig. 4F).

Regarding patellae without an apex (all of them with an orthograde body plan), we find a similar biomechanical behaviour between *Pongo* and *Pan* (which are two of the three anthropoids without a patellar apex). Stresses spread widely anteroposteriorly in these two taxa and maximum values (0.022 to 0.026 MPa) are concentrated in the posterior side and the distal areas of the patellae (Fig. 4H, I). This is similar to the pattern found in hylobatids (Fig. 4F, G) and *Homo* (Fig. 4K). Moreover, the highest stress values in *Pongo* and *Pan* during the first two phases of knee flexion are horizontally-oriented and this direction only changes during the full-flexed knee simulation. It must be noted that, in contrast, this pattern is different from the distribution observed in patellae with apex, which follow the direction of the applied force in the three stages of knee flexion as mentioned above. The patella of *Gorilla*, which is the other anthropoid whose patella does not have an apex (Fig. 4J), is instead mechanically very different to that of the remaining taxa (and not only to the orthograde great apes *Pongo* and *Pan*, but also to anthropoid monkeys, hylobatids and humans; see also Fig. 5). During all the phases of knee flexion, high stress values in *Gorilla* are exclusively concentrated in those regions

where forces are applied, ranging from 0.004 to 0.022 MPa in an extended-knee and from 0.008 to 0.026 MPa in semi- and fully-flexion. Thereby, overall, the patella of *Gorilla* shows broad stress-free areas during knee flexion (Fig. 4J).

In the case of the *Pierolapithecus* patella, patterns of stress distribution and stress magnitude are similar to those of extant *Pongo* and *Pan*, orthograde taxa with apex-less patellae (Fig. 4L). Maximum stress is distributed through the proximal and the distal half of the patella (mainly during the full-flexion phase), and is concentrated in the posterior side of the bone (thus reaching a maximum stress value of 0.026 MPa).

Experimental modification of the original geometries

A comparative analysis to determine the influence of the apex on patellar biomechanics was conducted by modifying three original 3D models (validation of the influence of subtle differences on apex morphology was also carried out; see Pina *et al.* 2019, appendices S3-5 for further explanation and results). We found that the effect of adding (in *Gorilla* and *Pongo*) or removing (in *Cercopithecus*) the apex in the original models induces substantial changes in von Mises stress results. The stress distribution in the modified model *Cercopithecus*-NoApex (Fig. 4M) strongly differs to that of the original (Fig. 4C)—being instead more similar to those of *Pongo* or *Pan* (Fig. 4H, I), and even *Homo* (Fig. 4K)—, since the distal part of the patella concentrates a greater amount of high stress (up to 0.026 MPa). On the other hand, results observed in the models of *Gorilla*-WApex (despite being different to any original model; Fig. 4O) and *Pongo*-WApex (Fig. 4N) are more similar to those of pronograde taxa with patellar apex from a mechanical point of view (e.g., *Cercopithecus* or *Mandrillus*; Fig. 4C, D). It is apparent that the distal end of the new models with patellar apex displays lower stress than the original model of *Pongo* (only reaching values of 0.012 MPa in the most distal region of

the added apex). Given that the original model of the gorilla patella shows a unique stress distribution (Fig. 4J), we elude to use it for comparisons. Moreover, the direction of the stress generated is different, being now (Fig. 4N, O) more similar to that of the force's vector than previously observed (Fig. 4H).

Quantitative results

All the variables inspected (Pina *et al.* 2019, appendix S2), except C30 (Shapiro-Wilk test p-value = 0.04; W = 0.85), follow a normal distribution (Shapiro-Wilk test p-value > 0.05). We evaluated whether the differences among groups according to Ap, BP, and BPAp are significant, and found no significant differences (p-value > 0.05) for all cases studied except three (p-value < 0.05; see below; Pina *et al.* 2019, appendix S6). At this point, it is important to note that the small sample size could tend to reduce the statistical power of the study and increases the margin of error. Cases in which differences are statistically significant are primates with or without apex at points D0.Ap and B60.Ap, and orthograde primates with apex *vs* orthograde primates without apex at D0.BPAp (Pina *et al.* 2019, appendix S6).

Figure 5 depicts the results of PCA for extant primates and *Pierolapithecus* comparing BPAp groups (loadings and eigenvalues in Pina *et al.* 2019, appendices S7, S8). Although we do not observe significant patterns in the data (Fig. 5), the two first components explain more than the 80% of the variance of the sample. MANOVA analyses corroborates the lack of differences among groups, since no statistical differences are found neither in PC1 nor in PC2 ($p > 0.05$ in the three stages of knee flexion). When PCs are analysed independently, only PC2 when the knee is completely extended shows significant differences among BPAp groups (ANOVA: p-value < 0.05, F = 4.82), specifically between orthograde primates with an apex (i.e., hylobatids and

humans) and orthograde primates without an apex (i.e., great apes; Tukey test p-value < 0.05).

DISCUSSION

Earlier works on Miocene apes stated that the morphology of the patella is related to the function of the knee (Harrison 1986; Ward *et al.* 1995; Pina *et al.* 2014*a*). The total proximodistal length of the patella, which is highly variable in living anthropoids depending on the presence/absence of a distal apex, is related to the torque of the knee joint (Harrison 1986; Ward *et al.* 1995). Considering this form-function relationship, it is logical to assume that those patellae without a distal apex (that is, those of great apes) correspond to a different biomechanical environment than those having this structure (i.e., non-great ape anthropoids). Our FE results on living anthropoids mostly failed to corroborate this hypothesis on qualitative terms, since stress distribution at the distal end and the posterior side in patellae with an apex belonging to pronograde anthropoids departs from those of geometries belonging to orthograde groups (i.e., patellae with or without apex; Fig. 4). However, we found some statistical differences at points D0 and B60 within the orthograde taxa, related to the presence (hylobatids and humans) or absence (great apes) of patellar apex (Pina *et al.* 2019, appendices S6, S7). Moreover, although clear patterns are not displayed in the PCA results, in an extended position of the knee, great apes (apex-less patellae) occupy their own morphospace (clearly in Fig. 5A; less in Fig. 5C). This differentiation is mainly driven by the weight of point D in PC2 (both in Fig. 5A and C), that is, the most distal point selected for analysis (just above the apex or the distal region in apex-less patellae). Interestingly, point D does not show differences when body plan types (BP) alone are compared; whereas if the variable “apex” is considered (individually, Ap, or together to body plan types, BPAp)

differences are found between patellae with and without apex (Pina *et al.* 2019, appendix S6). This fact suggests that such dissimilarities are due to the presence/absence of a distal apex. Thus, our results offer for the first time evidence of qualitative differences in stress distribution at the bone distal region within patellae belonging to pronograde and orthograde taxa (irrespective of the apex presence), when the knee is in an extended position. On the other hand, quantitative differences are found between taxa with patellae with or without an apex (irrespective of their body plan). We could conclude that, while orthograde taxa patellae similarly distribute stress during knee flexion, the magnitude of this stress (quantitatively) differs if the patellae have a distal apex or not. Despite the difficulty of clearly decoupling body plan types (pronogrady-orthogrady) from specific locomotor behaviours (mainly those types associated with an antipronograde body plan), our FE results are underpinned by biomechanical and gait similarities among anthropoid taxa. Thus, the apex seems to participate in stress dissipation through the whole patella in pronograde quadrupeds, as the most distal region of the bone remains less stressed or stress-free (Fig. 4A-E). Interestingly, this biomechanical role is confirmed by the results obtained for the modified models. When an apex is virtually added to the patellae of an extant orangutan and gorilla (Fig. 4N, O), stress patterns show clear affinities with pronograde primates (e.g., *Cercopithecus* and *Colobus*), for which the most distal part of the apex is free of stress in every tested stage of knee flexion. On the other hand, when the apex is virtually removed in *Cercopithecus*, this favours the appearance of high stress at the most distal part of the apex (mainly during semi-flexion and full flexion; Fig. 4M), similar to the patterns obtained for orangutans and chimpanzees (and orthogrades with an apex such as humans).

The patella of *Pierolapithecus* biomechanically resembles those of extant great apes (patellae without an apex), that is, chimpanzees and orangutans (but not gorillas). This fact suggests similar locomotion performance (habitual knee positions and preferential direction of movements) and/or body weight loading and transmission in both *Pierolapithecus* and great apes under a human-like knee model. However, due to the nature of our work, we cannot provide direct biomechanical inferences for the knee of *Pierolapithecus*, since its patellar response under other primate models could vary. Nonetheless, as above-commented, previous authors linked the external morphology of the patella to the function of the knee (Harrison 1986; Ward *et al.* 1995). Pina *et al.* (2014*a*) reported that the patellar shape in *Pierolapithecus* resembles that of great apes and our FE results support this idea, as well as the fact that patellar shape and function in living anthropoids are strongly related (see subsection *Experimental modification of the original geometries*). Hence, our FE results suggest that *Pierolapithecus* displayed not only a great ape-like patellar morphology, but also non-*Gorilla* great ape-like knee biomechanics (under a human-knee model). Given that the only preserved evidence for the *Pierolapithecus* knee is the patella, we might relate the morpho- and biomechanical resemblances of this bone with a habitual extended and a versatile knee as seen in great apes, that is, the joint would be able to move in ways other than in the parasagittal plane as occurs in living quadrupeds (Martin 1990; Hunt 1991, 2004; Madar *et al.* 2002; Crompton 2016). As earlier works remarked, locomotor repertoires including antipronograde behaviours (e.g., vertical climbing, clambering, and suspension) require a combination of versatile movements of the joints. These needs are particularly strong at the knee joint, since it moves in different directions during active locomotion and supports a non-stereotyped set of loads coming from both muscles and body weight (Martin 1990; Hunt 1991, 2004; Madar *et al.* 2002; Fleagle 2013; Crompton 2016).

Additionally, based on comparative results of the patellar mediolateral breadth in mammals, Haxton (1944) proposed that the most relevant role of the patella occurs when the knee is extended. Remarkably, our statistical results also highlight this fact, showing differences between taxa with patellae with or without an apex in an extended knee phase. Using a human-like knee model, we found differences between the group of hylobatids and humans, and great apes. This fact suggests that the use of the knee in an extended position, when compression loads are supported (Stern 1975), is different among orthograde hominoids despite their shared body plan. Such differences might be due to the frequency they rely on different types of locomotion and the different biomechanical requirements of each of these locomotor types. Humans habitually use an extended position of the knee during bipedalism, whereas great apes use the hind limb in compression mostly during clambering and vertical climbing, and knuckle-walking in the case of African apes (Stern 1975; Sugardjito 1982; Madar *et al.* 2002; Hunt 2004; Crompton 2016). Hylobatids spend most of the time suspended and/or brachiating (50-80%; Fleagle 1980; Vereecke *et al.* 2006; Fan *et al.* 2013, among others), meaning that their hind limb is barely used under compressive loads. Hence, in this case, the stress distribution similarities with other hominoids are more difficult to explain. Nonetheless, hylobatids' patellar shape shows some affinities with those of stem hominoids such as *Ekembo* (Pina *et al.* 2014*a*), whose patellar shape could represent the hominoid ancestral morphology (Ward *et al.* 1995). This stem hominoid already relied on a non-specialized locomotor repertoire (e.g., Ward 2015), which could be reflected in its knee biomechanics. Although hylobatids mainly rely on suspensory behaviours, they are able to perform a wide variety of locomotor types and its biomechanical response, as in *Ekembo*, might be indicative of a non-specialized knee

performance under compression loads. Nonetheless, further analyses are needed to corroborate this hypothesis.

We propose that the stress distribution resemblances between *Pierolapithecus* and great apes patellae might be due to a substantial amount of extended positions of the knee during (non-bipedal) locomotion, thus confirming the importance of some kind of antipronograde positional behaviour within this Miocene hominoid locomotor repertoire. On the other hand, the biomechanical response to knee flexion in the patella of *Pierolapithecus* clearly departs from those of pronograde quadrupedal primates. Although the degree of above-branch quadrupedalism inferred for this Miocene taxon would probably be considerable (Moyà-Solà *et al.* 2004, Almécija *et al.* 2009; Alba 2012), we cannot confirm this hypothesis on the basis of our FE results. In the same line, as suspensory taxa in our patellar sample (orangutans, hylobatids, and spider monkeys) do not show any qualitative or quantitative distinctiveness, our results do not allow us to confirm (after Begun and Ward 2005; Deane and Begun 2008, 2010) and/or discard (after Moyà-Solà *et al.* 2004, 2005; Almécija *et al.* 2009; Alba *et al.* 2010) the presence of suspensory behaviours within the *Pierolapithecus* locomotor repertoire. Our results, together with most of the anatomical evidence available for *Pierolapithecus*, advocate for a frequent use of vertical climbing (Moyà-Solà *et al.* 2004, 2005; Almécija *et al.* 2009; Alba *et al.* 2010; Pina *et al.* 2014*a*). Thus, we could hypothesize that specific positional and loading conditions of the knee joint may have been functionally relevant for the origin of particular antipronograde locomotor modes such as vertical climbing (and probably clambering and suspension) in the first orthograde hominid forms. Moreover, this scenario would also support the hypothesis that vertical climbing (instead of below-branch suspension) might be the main driver of locomotor evolution

in these early orthograde taxa (Moyà-Solà *et al.* 2004; Alba 2012; Pina *et al.* 2014*a*; Grabowski & Jungers 2017).

CONCLUSIONS

The middle Miocene hominoid *Pierolapithecus catalaunicus* is the first unquestionable orthograde taxon in the primate fossil record. Earlier works suggested that this species would show a unique mixture of primitive (above-branch quadrupedalism) and derived (antipronograde behaviours, probably vertical climbing) locomotor types within its locomotor repertoire. It has been corroborated in the last decades, that Miocene taxa displayed positional behaviours currently unknown. However, a better comprehension of these unique combinations and their relationship with bone morphology and biomechanics will allow us to unravel questions related to the origin of the specialized antipronograde behaviours observed in living apes and humans, including terrestrial bipedalism. In-depth studies of Miocene taxa postcranial morphology and biomechanics are indispensable to address these questions. In this work, we investigate the biomechanical response of the *Pierolapithecus* knee through FEA, comparing this taxon with a large sample of extant anthropoids (analysed using this methodology for the first time, except in the case of humans). *Pierolapithecus* patellar stress distribution shows similarities with great apes (except gorillas). These results support those obtained for its patellar morphology, suggesting that the knee of *Pierolapithecus* was similar to that of great apes in terms of both morphology and biomechanics. Given that our analyses show that von Mises stress distribution is different between living pronograde and orthograde taxa, and moreover differences are also found within orthograde taxa (depending on the presence/absence of patellar apex), we could exclude a pronograde quadrupedal-like and an orthograde human bipedal-like biomechanical response to knee

flexion in the *Pierolapithecus* patella. This fact supports the idea that some novel antipronograde positional behaviour would be performed by this taxon, being most probably vertical climbing on the basis of present anatomical evidence (including its patellar shape). Assuming this, vertical climbing seems to have played an important role in the origin and evolution of the hominoids' orthograde-related behaviours, including human bipedalism. This locomotor mode might be the main driver in the evolutionary pathway of hominoid locomotion against below-branch suspension, as some authors previously proposed for the hominid's last common ancestor and subsequent evolutionary stages.

Acknowledgements. This work has been supported by the Spanish Agencia Estatal de Investigación-European Regional Developmental Fund (CGL2016-76431-P, and CGL2017-82654-P MINECO/FEDER, EU), the Generalitat de Catalunya (CERCA Programme), the Japan Society for the Promotion of Science (P17394 JSPS International Research Fellowship grant to M.P.) and The L.S.B. Leakey Foundation (to M.P.). J.M-N. was supported by the Deutsche Forschungsgemeinschaft (DFG, German Research Foundation, KA 1525/9-2). S.M.S. is member of the consolidated research groups 2017 SGR 086 of the Generalitat de Catalunya. Authors would thank Pere Ibáñez for kindly providing some 3D virtual models of extant patellae. We also thank Eileen Westwig (American Museum of Natural History, New York), and Judy Chupasko and Mark Omura (Museum of Comparative Zoology-Harvard University, Cambridge) for access to museum collections. Part of the CT-scans included in this work were performed at the Center for Nanoscale Systems (CNS), a member of the National Nanotechnology Infrastructure Network (NNIN), which is supported by the

National Science Foundation under NSF award no. ECS-0335765. CNS is part of Harvard University.

DATA ARCHIVING STATEMENT

Data for this study are available in the [Dryad Digital Repository]: https://datadryad.org/review?doi=doi:10.5061/dryad.453dg14

DATA AVAILABILITY STATEMENT

The data that support the findings of this study are available from the corresponding author upon request. 3D surface models and CAD objects are also available at MorphoSource.

REFERENCES

ALBA, D. M. 2012. Fossil apes from the Vallès-Penedès basin. *Evolutionary Anthropology*, **21**, 254–269.

— ALMÉCIJA, S., DEMIGUEL, D., FORTUNY, J., DE LOS RÍOS, M. P., PINA, M., ROBLES, J. M. and MOYÀ-SOLÀ, S. 2015. Miocene small-bodied ape from Eurasia sheds light on hominoid evolution. *Science*, **350**(6260), aab2625.

— ALMÉCIJA, S. and MOYÀ-SOLÀ, S. 2010. Locomotor inferences in *Pierolapithecus* and *Hispanopithecus*: Reply to Deane and Begun (2008). *Journal of Human Evolution*, **59**, 143–149.

— CASANOVAS-VILAR, I., GARCÉS, M., ROBLES, J. M. 2017. Ten years in the dump: An updated review of the Miocene primate-bearing localities from Abocador de Can Mata (NE Iberian Peninsula). *Journal of Human Evolution*, **102**, 12–20.

ALMÉCIJA, S. ALBA, D. M. and MOYÀ-SOLÀ, S. 2009. *Pierolapithecus* and the functional morphology of Miocene ape hand phalanges: paleobiological and evolutionary implications. *Journal of Human Evolution*, **57**, 284–297.

BADOUX, D. M. 1974. An introduction to biomechanical principles in primate locomotion and structure. 1–43. *In* JENKINS, F. A. (ed.). *Primate Locomotion.* New York, Academic Press, 402 pp.

BEGUN, D. R. 2009. Dryopithecins, Darwin, de Bonis, and the European origin of the African apes and human clade. *Geodiversitas,* **31**, 789–816.

— 2015. Fossil record of Miocene hominoids. 1261–1332. *In* HENKE, W., and TATTERSALL, I. (eds.). *Handbook of Paleoanthropology, 2nd ed*. Springer, Heidelberg, 2624 pp.

— and WARD, C. V. 2005. Comment on "*Pierolapithecus catalaunicus*, a new Middle Miocene great ape from Spain". *Science*, **208**, 203c.

BRIGHT, J. A., 2014. A review of paleontological finite element models and their validity. *Journal of Paleontology,* **88**, 760–769.

CARTMILL, M. 1985. Climbing. 73–88. *In* HILDEBRAND, M., BRAMBLE, D., LIEM, K. and WAKE, D. (eds). *Functional Vertebrate Morphology*. Cambridge, Belknap Press, 430 pp.

CASANOVAS-VILAR, I., ALBA, D. M., GARCÉS, M., ROBLES, J. M. and MOYÀ-SOLÀ, S. 2011. Updated chronology of the Miocene hominoid radiation in Western Eurasia. *Proceedings of the National Academy of Sciencies USA,* **108**, 5554–5559.

CAZENAVE, M., OETTLÉ, A., THACKERAY, J. F., NAKATSUKASA, M., DE BEER, F., HOFFMAN, J. and MACCHIARELLI, R. 2019. The SKX 1084 hominin patella from Swartkrans Member 2, South Africa: An integrated

analysis of its outer morphology and inner structure. *Comptes Rendus Palevol*, **18**, 223–235.

CROMPTON, R. H. 2016. The hominins: a very conservative tribe? Last common ancestors, plasticity and ecomorphology in Hominidae. Or, what's in a name? *Journal of Anatomy*, **228**, 686–699.

— SELLERS, W. I. and THORPE, S. K. S. 2010. Arboreality, terrestriality and bipedalism. *Philosophical Transactions of the Royal Society B*, **365**, 3301–3314.

DEANE, A. S. and BEGUN, D. R. 2008. Broken fingers: retesting locomotor hypotheses for fossil hominoids using fragmentary proximal phalanges and high-resolution polynomial curve fitting (HR-PCF). *Journal of Human Evolution*, **55**, 691–701.

— 2010. *Pierolapithecus* locomotor adaptations: a reply to Alba et al.'s comment on Deane and Begun (2008). *Journal of Human Evolution*, **59**, 150–154.

DEMIGUEL, D., AZANZA, B., CEGOÑINO, J., RUÍZ, I. and MORALES, J. 2015. The interplay between increased tooth crown-height and chewing efficiency, and implications for Cervidae evolution. *Lethaia*, **49**, 117–129.

DOBLARÉ, M., GARCÍA, J. M. and GÓMEZ, M. J. 2004. Modelling bone tissue fracture and healing: a review. *Engineering Fracture Mechanics*, **71**, 1809–1840.

DUMONT, E. R., PICCIRILLO, J., GROSSE, L. R. 2005. Finite-element analysis of biting behavior and bone stress in the facial skeletons of bats. *The Anatomical Record Part A: Discoveries in Molecular, Cellular, and Evolutionary Biology*, **283A**, 319–330.

DUMONT, E. R., GROSSE, I. R. and SLATER, G. J. 2009. Requirements for comparing the performance of finite element models of biological structures. *Journal of Theoretical Biology*, **256**, 96–103.

FAN, P., SCOTT, M. B., FEI, H. and MA, C. 2013. Locomotion behavior of cao vit gibbon (*Nomascus nasutus*) living in karst forest in Bangliang Nature Reserve, Guangxi, China. *Integrative Zoology*, **8**, 356–364.

FITTON, L. C., PRÔA, M., ROWLAND, C., TORO-IBACACHE, V. and O'HIGGINS, P. 2015. The impact of simplifications on the performance of a Finite Element Model of a *Macaca fascicularis* cranium. *The Anatomical Record*, **298**, 107–121.

FLEAGLE, J. G. 1976. Locomotion and posture of the Malayan siamang and implications for hominoid evolution. *Folia primatologica*, **26**, 245–269.

— 1980. Locomotion and posture. 191–207. *In* CHIVERS, D. J. (ed.) *Malayan Forest Primates: Ten Year's Study in Tropical Rain Forest*. Plenum Press, New York, pp. Custom 7.

— 2013. *Primate Adaptation and Evolution*. Academic Press, San Diego, 436 pp.

FORTUNY, J., MARCÉ-NOGUÉ, J., HEISS, E., SANCHEZ, M., GIL, L. and GALOBART, À. 2015. 3D bite modeling and feeding mechanics of the largest living amphibian, the Chinese giant salamander *Andrias davidianus* (Amphibia: Urodela). *PLOS ONE*, **10**, e0121885.

FORTUNY, J., MARCÉ-NOGUÉ, J., DE ESTEVAN-TRIVIGNO, S., MUJAL, E. and GIL, L. 2016. Comparative 3D analyses and palaeoecology of giant early amphibians (Temnospondyli: Stereospondyli). *Scientific Reports*, **6**, 30387.

GODINHO, R. M., TORO-IBACACHE, V., FITTON, L. C. and O'HIGGINS, P. 2017. Finite element analysis of the cranium: Validity, sensitivity and future directions. *Comptes Rendus Palevol*, **16**, 600–612.

GRABOWSKI, M. and JUNGERS, W. L. 2017. Evidence of a chimpanzee-sized ancestor of humans but a gibbon-sized ancestor of apes. *Nature Communications*, **8**(1), 880.

GRÖNING, F., FAGAN, M. and O'HIGGINS, P. 2013. Comparing the distribution of strains with the distribution of bone tissue in a human mandible: A Finite Element Study. *The Anatomical Record*, **296**, 9–18.

GIL, L., MARCÉ-NOGUÉ, J., and SÁNCHEZ, M. 2015. Insights into the controversy over materials data for the comparison of biomechanical performance in vertebrates. *Palaeontologica Electronica*, **18.1.12A**, 1–24.

HAMMOND, A. S., ALBA, D. M., ALMÉCIJA, S. and MOYÀ-SOLÀ, S. 2013. Middle Miocene *Pierolapithecus* provides a first glimpse into early hominid pelvix morpholgy. *Journal of Human Evolution*, **64**, 658–666.

HARRISON, T. 1986. A reassessment of the phylogenetic relationships of *Oreopithecus bambolii* Gervais. *Journal of Human Evolution*, **15**, 541–583.

HAXTON, H. 1944. The patellar index in mammals. *Journal of Anatomy*, **78**, 106–107.

HEEGAARD, J., LEYVRAZ, P. F., CURNIER, A., RAKOTOMANANA, L. and HUISKES, R. 1995. The biomechanics of the human patella during passive knee flexion. *Journal of Biomechanics*, **28**, 1265–1279.

HOUNSFIELD, G. N. 1973. Computerized transverse axial scanning (tomography). Part I. Description of system. *The British Journal of Radiology*, **46**, 1016–1022.

— 1976. Historical notes on computerized axial tomography. *Journal of the Canadian Association of Radiologists,* **27**, 135–142.

HUNT, K. D. 1991. Positional behavior in the Hominoidea. *International Journal of Primatology,* **12**, 95–118.

— 1992. Positional behavior of *Pan troglodytes* in the Mahale Mountains and Gombe Stream National Parks, Tanzania. *American Journal of Physical Anthropology*, **87**, 83–105.

— 2004. The special demands of great ape locomotion and posture. 172– 189. *In* RUSSON, A. E. and BEGUN, D. R. (eds). *The Evolution of Though Evolutionary Origins of Great Ape Intelligence.* New York, Cambridge University Press. 396 pp.

— 2016. Why are there apes? Evidence for the co-evolution of ape and monkey ecomorphology. *Journal of Anatomy,* **228**, 630–685.

— CANT, J., GEBO, D., ROSE, M., WALKER, S., and YOULATOS, D. 1996. Standardized descriptions of primate locomotor and postural modes. *Primates*, **37**, 363–387.

KELLEY, J. 1997. Paleobiological and phylogenetic significance of life history in Miocene hominoids. 173–208. *In* Begun, D. R., WARD, C. V. and ROSE, M. D. (eds). *Function, Phylogeny, and Fossils: Miocene Hominoid Evolution and Adaptations.* New York, Plenum Press, 424 pp.

LARSON, S. G. 1998. Parallel evolution in the hominoid trunk and forelimb. *Evolutionary Anthropology,* **6**, 87–99.

LOVEJOY, C. O. 2005. The natural history of human gait and posture. Part 2. Hip and thigh. *Gait & Posture*, **21**, 113–124.

— 2007. The natural history of human gait and posture: Part 3. The knee. *Gait & Posture,* **25**, 325–341.

MCHENRY, C. R., CLAUSEN, P. D., DANIEL, W. J., MEERS, M. B., and PENDHARKAR, A. 2006. Biomechanics of the rostrum in crocodilians: A comparative analysis using finite-element modeling. *The Anatomical Record Part A: Discoveries in Molecular, Cellular, and Evolutionary Biology,* **288**, 827–849.

MADAR, S. I., ROSE, M. D., KELLEY, J., MACLATCHY, L. and PILBEAM, D. 2002. New *Sivapithecus* postcranial specimens from the Siwaliks of Pakistan. *Journal of Human Evolution,* **42**, 705–752.

MARCÉ-NOGUÉ, J., FORTUNY, J., GIL, L. and GALOBART, A. 2011. Using reverse engineering to reconstruct tetrapod skulls and analyse its feeding behaviour. Paper 237. *In* TOPPING, B. H. V. and TSOMPANAKIS, Y. (eds). *Proceedings of the Thirteenth International Conference on Civil, Structural and Environmental Engineering Computing.* Civil-Comp Press, Stirlingshire, 122 pp.

MARCÉ-NOGUÉ, J., DEMIGUEL, D., DE ESTEBAN-TRIVIGNO, S., FORTUNY, J. and GIL, L. 2013. Quasi-homothetic transformation for comparing the mechanical performance of planar models in biological research. *Palaeontologica Electronica,* **16**, 6T, 15 p.

MARCÉ-NOGUÉ, J., FORTUNY, J., GIL, L. and SÁNCHEZ, M. 2015. Improving mesh generation in finite element analysis for functional morphology approaches. *Spanish Journal of Palaeontology,* **30**, 117–132.

MARTIN, R. D. 1990. *Primate Origins and Evolution. A Phylogenetic Reconstruction*. Princeton University Press, Princeton, 840 pp.

MASOUROS, S. D., BULL, A. M. J. and AMIS, A. A. 2010. (i) Biomechanics of the knee joint. *Orthopaedics and Trauma,* **24**, 84–91.

MCGRAW, W. S. 1996. Cercopithecid locomotion, support use, and support availability in the Tai Forest, Ivory Coast. *American Journal of Physical Anthropology*, **100**, 507–522.

— 1998. Posture and support use of Old World monkeys (Cercopithecidae): The influence of foraging strategies, activity patterns, and the spatial distribution of preferred food items. *American Journal of Primatology*, **46**, 229–250.

MOYÀ-SOLÀ, S. and KÖHLER, M. 1996. A *Dryopithecus* skeleton and the origin of great-ape locomotion. *Nature,* **379**, 156–159.

MOYÀ-SOLÀ, S., KÖHLER, M., ALBA, D. M., CASANOVAS-VILAR, I. and GALINDO, J. 2004. *Pierolapithecus catalaunicus* a new Middle Miocene great ape from Spain. *Science*, **306**, 1339–1344.

MOYÀ-SOLÀ, S., KÖHLER, M., ALBA, CASANOVAS-VILAR, I. and GALINDO, J. 2005. Response to comment on "*Pierolapithecus catalaunicus*, a new Middle Miocene great ape from Spain". *Science*, **308**, 203d.

NISELL, R. 1985. Mechanics of the knee. A study of joint and muscle load with clinical applications. *Acta orthopaedica Scandinavica,* **Suppl. 216**, 1–42.

OHMAN, J. C., KROCHTA, T. J., LOVEJOY, C. O., MENSFORTH, R. P. and LATIMER, B. 1997. Cortical bone distribution in the femoral neck of hominoids: Implications for the locomotion of *Australopithecus afarensis*. *American Journal of Physical Anthropology*, **104**, 117–131.

OXNARD, C. E. 1971. Tensile forces in skeletal structures. *Journal of Morphology*, **134**, 425–436.

PÉREZ DE LOS RÍOS, M., MOYÀ-SOLÀ, S. and ALBA, D. M. 2012. The nasal and paranasal architecture of the Middle Miocene ape *Pierolapithecus catalaunicus* (primates: Hominidae): Phylogenetic implications. *Journal of Human Evolution*, **63**, 497–506.

PINA, M. 2016. Unravelling the positional behaviour of fossil hominoids: Morphofunctional and structural analysis of the primate hindlimb. Universitat Autònoma de Barcelona.

— ALBA, D. M., ALMÉCIJA, S., FORTUNY, J. and MOYÀ-SOLÀ, S. 2012. Brief communication: Paleobiological inferences on the locomotor repertoire of extinct hominoids based on femoral neck cortical thickness: The fossil great ape *Hispanopithecus laietanus* as a test-case study. *American Journal of Physical Anthropology*, **149**, 142-148.

— ALMÉCIJA, S., ALBA, D. M., O'NEILL, M. C. and MOYÀ-SOLÀ, S. 2014*a*. The Middle Miocene ape *Pierolapithecus catalaunicus* exhibits extant great ape-like morphometric affinities on its patella: inferences on knee function and evolution. *PLOS ONE*, **9**(3), e91944.

— ALMÉCIJA, S., ALBA, D. M. and MOYÀ-SOLÀ, S. 2014b. Disentangling the positional behavior of European Miocene hominoids: evidence from the internal structure of the femoral neck 124. *In* DELFINO, M., CARNEVALE, G. and PAVIA, M. (eds). *12th Annual Meeting of Vertebrate Paleontologists*. Torino, Italy.

— DEMIGUEL, D., PUIGVERT, F., MARCÉ-NOGUÉ, J. and MOYÀ-SOLÀ, S. 2019. Data from: Knee function through Finite Element Analysis and the role of Miocene hominoids to understand the origin of antipronograde behaviours: the

Pierolapithecus catalaunicus' patella as a test-case study. *Dryad Digital Repository*. http://doi.org/10.5061/dryad.453dg14

PLATZER, W. 2008. *Color Atlas of Human Anatomy. Locomotor System*. Thieme, Stuttgart (Germany), 468 pp.

POLK, J. D. 2002. Adaptive and phylogenetic influences on musculoskeletal design in cercopithecine primates. *Journal of Experimental Biology*, **205**, 3399–3412.

— WILLIAMS, S. A. and PETERSON, J. V. 2009. Body size and joint posture in primates. *American Journal of Physical Anthropology*, **140**, 359–367.

PREUSCHOFT, H. 1970. Functional anatomy of the lower extremity. 221–294. *In* BOURNE, G. (ed.). *The Chimpanzee*. Karger, Basel/München/New York, 468 pp.

— 2004. Mechanisms for the acquisition of habitual bipedality: are there biomechanical reasons for the acquisition of upright bipedal posture? *Journal of Anatomy*, **204**, 363–384.

— and WITZEL, U. 2002. Biomechanical investigations on the skulls of reptiles and mammals. *Senckenbergiana Lethaea*, **82**, 207–222.

R CORE TEAM. 2017. R: A language and environment for statistical computing. R Foundation for Statistical Computing, Vienna, Austria.

RAYFIELD, E. J. 2007. Finite element analysis and understanding the biomechanics and evolution of living and fossil organisms. *Annual Review of Earth and Planetary Sciences*, **35**, 541–576.

ROSE, M. D. 1983. Miocene hominoid postcranial morphology. Monkey-like, ape-like, neither, or both? 503–516. *In* CIOCHON, R. L. and CORRUCCINI, R. S. (eds). *New Interpretations of Ape and Human Ancestry*. Plenum Press, New York, pp. Custom 7.

SAMUELS, M. E., REGNAULT, S. and HUTCHINSON, J. R. 2017. Evolution of the patellar sesamoid bone in mammals. *PeerJ*, **5**, e3103.

SCHINDLER, O. S. and SCOTT, W. N. 2011. Basic kinematics and biomechanics of the patello-femoral joint. Part 1: The native patella. *Acta Orthopaedica Belgica*, **77**, 421–431.

SENUT, B. 2016. Morphology and environment in some fossil Hominoids and Pedetids (Mammalia). *Journal of Anatomy*, **228**, 700–715.

SERRANO-FOCHS, S., DE ESTEBAN-TRIVIGNO, S., MARCÉ-NOGUÉ, J., FORTUNY, J. and FARIÑA, R. A. 2015. Finite element analysis of the Cingulata jaw: An ecomorphological approach to armadillo's diets. *PLOS ONE*, **10**(4), e0120653.

SHARP, A. C. 2015. Comparative finite element analysis of the cranial performance of four herbivorous marsupials. *Journal of Morphology*, **276**, 1230–1243.

SCHINDLER, O. S. and SCOTT, W. N. 2011. Basic kinematics and biomechanics of the patello-femoral joint. Part 1: The native patella. *Acta Orthopaedica Belga*, **77**, 421–431.

SMITH, R. J. and JUNGERS, W. L. 1997. Body mass in comparative primatology. *Journal of Human Evolution*, **32**, 523–559.

STERN, J. T. Jr. 1975. Before bipedality. *Yearbook of Physical Anthropology*, **19**, 59–68.

SUGARDJITO J. 1982. Locomotor behaviour of the Sumatran orang-utan *(Pongopygmaeus abelii)* at Ketambe, Gunung Leuser National Park. *Malayan Nature Journal*, **35**, 57–64.

SUSANNA, I., ALBA, D. M., ALMÉCIJA, S. and MOYÀ-SOLÀ, S. 2010*a*. The lumbar vertebrae of the Middle Miocene stem great ape ape *Pierolapithecus catalaunicus* (Primates: Hominidae). *Cidaris,* **30**, 311–316.

— 2010*b*. The lumbar vertebrae of the Middle Miocene stem great ape *Pierolapithecus catalaunicus* (Primates: Hominidae). *American Journal of Physical Anthropology,* **141**(S50), 227.

TORO-IBACACHE, V., FITTON, L. C., FAGAN, M. J. and O'HIGGINS, P. 2016. Validity and sensitivity of a human cranial finite element model: implications for comparative studies of biting performance. *Journal of Anatomy*, **228**, 70–84.

TSENG, Z. J. and FLYNN, J. J. 2014. Convergence analysis of a finite element skull model of *Herpestes javanicus* (Carnivora, Mammalia): implications for robust comparative inferences of biomechanical function. *Journal of Theoretical Biology*, **365**, 112–148.

VEREECKE, E. E., D'AOÛT, K. and AERTS, P. 2006. Locomotor versatility in the white-handed gibbon (*Hylobates lar*): a spatiotemporal analysis of the bipedal, tripedal, and quadrupedal gaits. *Journal of Human Evolution,* **50**, 552–567.

WARD, C. V. 2015. Postcranial and Locomotor Adaptations of Hominoids. 1363–1386. *In* HENKE, W. and TATTERSALL, I. (eds). *Handbook of Paleoanthropology*. Springer, Berlin Heidelberg, pp. Custom 7.

— RUFF, C. B., WALKER, A., TEAFORD, F., ROSE, M. D. and NENGO, I. O. 1995. Functional morphology of *Proconsul* patellas from Rusinga Island, Kenya, with implications for other Miocene-Pliocene catarrhines. *Journal of Human Evolution*, **29**, 1–19.

YOULATOS, D. 2002. Positional behavior of black spider monkeys (*Ateles paniscus*) in French Guiana. *International Journal of Primatology,* **23**, 1071–1093.

FIGURES CAPTIONS

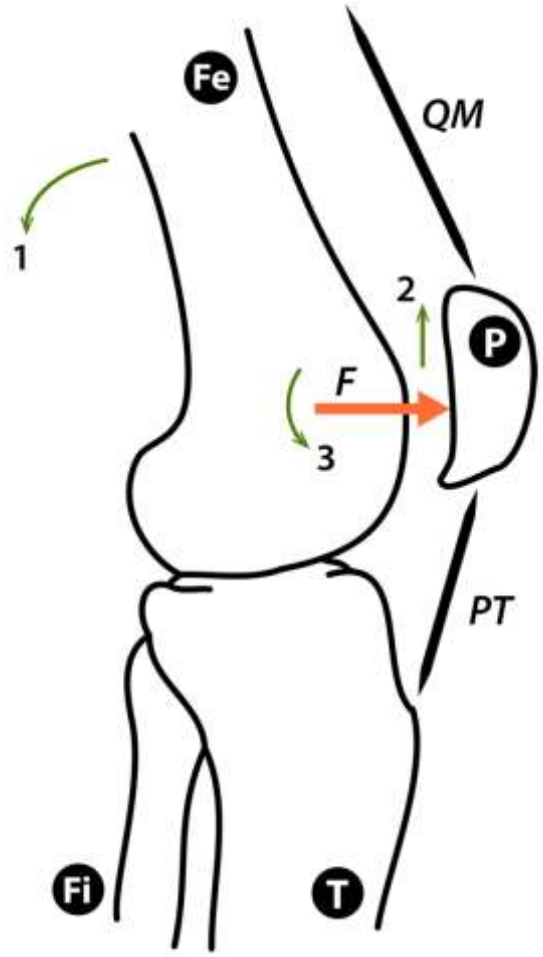

Fig. 1. Schematic representation of the knee kinematic model used to perform the Finite Element Analyses in this study (see 'Material and methods' for a more comprehensive description of the model). The patella (P) is constrained by the quadriceps muscle (QM) and patellar tendon (PT) areas of attachment (see text for further explanation). Contact between the femur (Fe) and the patella generates a force (F). This force acts in the distal part of the articular surface of the patella when the knee is extended. When the joint flexes (1), the force (contact) moves proximally (2) and its angle of actions changes (3). Fi, fibula; T, tibia.

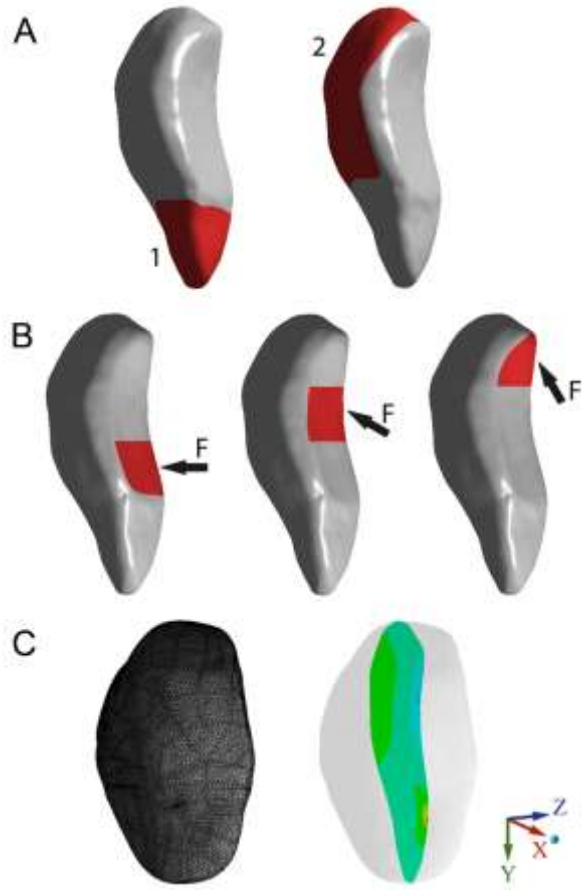

Fig. 2. Pre-processing of patellar 3D models for Finite Element Analysis. 3D models of primate patellae were transformed to CAD (Computer-Aided Design) objects (see SI Appendix S1) to implement the model depicted in Fig. 1 and extensively explained in the text. **A**, In every CAD model boundary conditions were applied: 1, patellar tendon attachment area; and 2, quadriceps muscle attachment area. **B**, The force (F) was applied in different areas and with different directions (black arrows) that represent three steps of knee flexion (joint extended, left; semi-flexed knee, centre; full-flexed knee, right). **C**, Finally, a sagittal image in the mediolateral midpoint (right) of each patellar model (left) was selected for comparison.

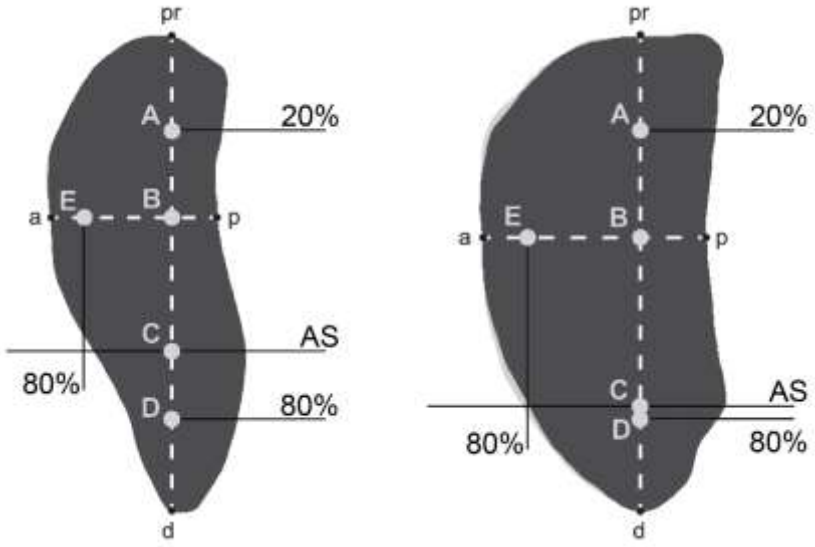

Fig. 3. Set of points (A-E) selected in the anthropoid sample for quantitative analysis of von Mises stress distribution in patellae with apex (left) and patellae without apex (right). In order to obtain the points, the maximum proximodistal height (pr-d) and anteroposterior width (a-p) were drawn. Then, points were defined as follows: A, 20% of the total pr-d length from the proximal end (pr); B, intersection between pr-d and a-p; C, intersection between pr-d and the horizontal line at the base of the articular surface (AS); D, 80% of the total pr-d length from the proximal end (pr); and E, 80% of the total a-p length from the posterior side (p).

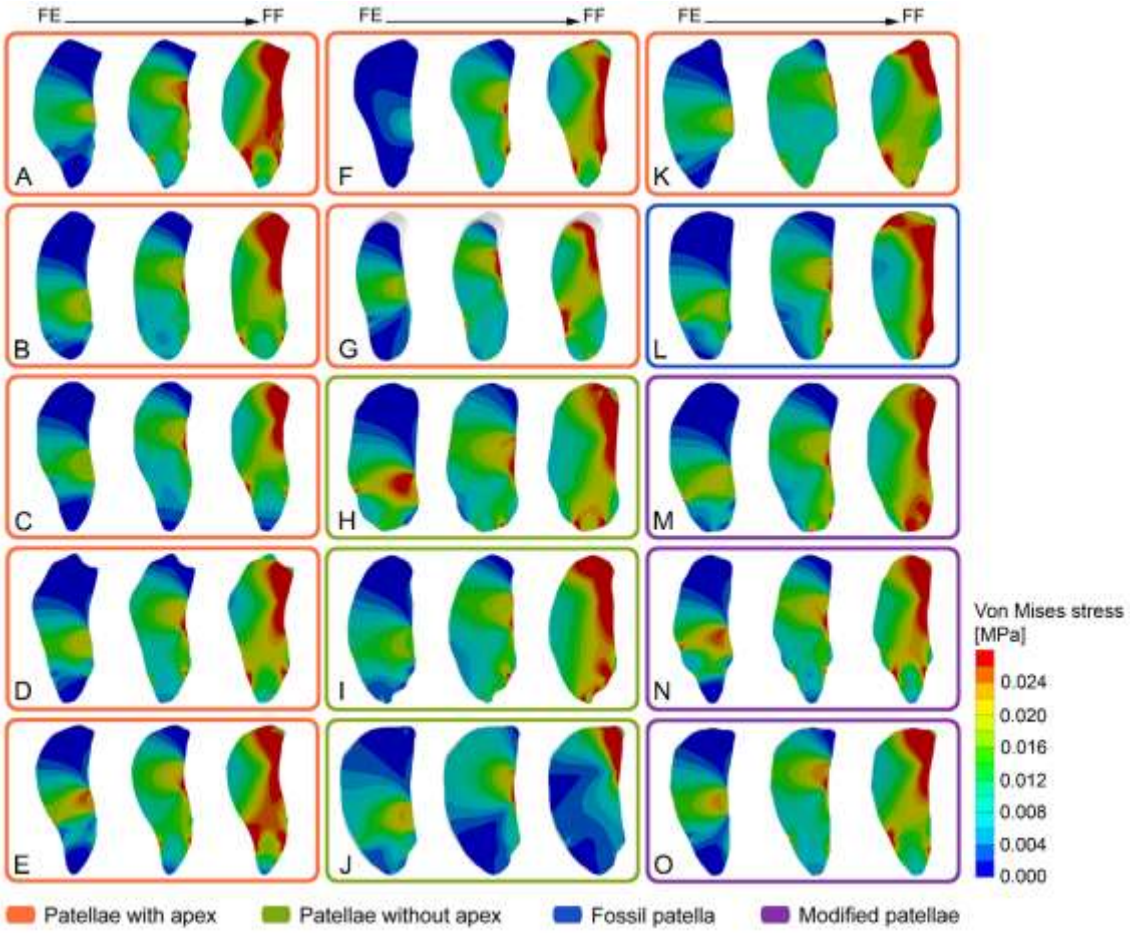

Fig. 4. Von Mises stress distribution (in MPa) in the mid-sagittal section (top, superior; left, posterior) of the patellae of extant anthropoids (**A-K**), the fossil great ape *Pierolapithecus catalaunicus* (**L**), and the modified patellar models (**M-O**) during extended (left), semi-flexed (middle), and full-flexed (right) knee phases. **A**, *Cebus*; **B**, *Ateles*; **C**, *Cercopithecus*; **D**, *Mandrillus*; **E**, *Colobus*; **F**, *Hylobates*; **G**, *Symphalangus*; **H**, *Pongo*; **I**, *Pan*; **J**, *Gorilla*; **K**, *Homo*; **L**, *Pierolapithecus*; **M**, *Cercopithecus*-NoApex; **N**, *Pongo*-WApex; and **O**, *Gorilla*-WApex. Results homogenized according to the same stress scale (minimum = 0 MPa; maximum = 0.026 MPa). Abbreviations: FE, fully-extended knee; FF, fully-flexed knee.

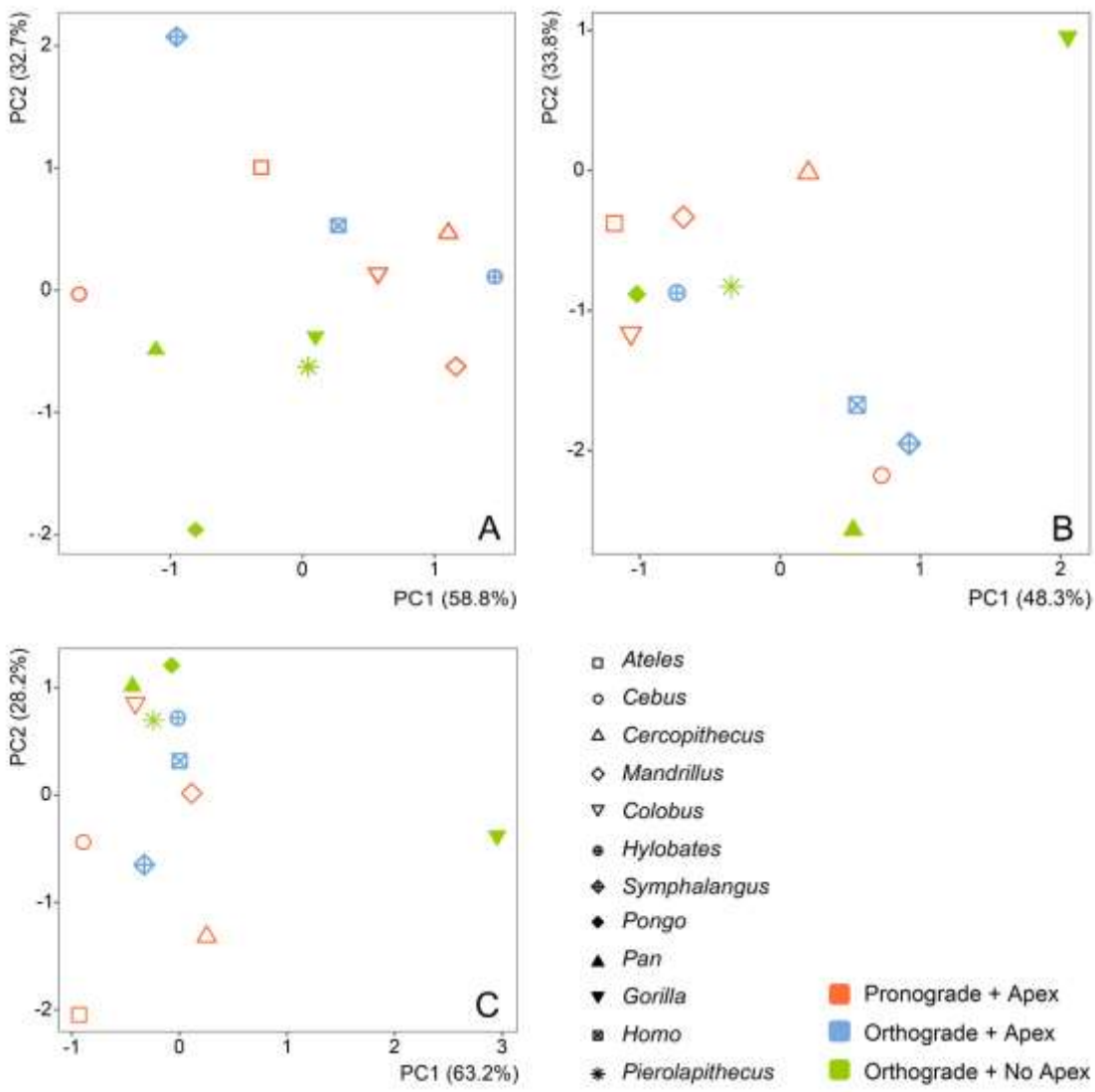

Fig. 5. Principal Component Analysis (PCA) results. Plots of the two first principal components (PC) for the set of points selected in the midsagittal slice of the patellar sample. PCA were performed for every stage of knee flexion: **A**, extended; **B**, semi-flexed; **C**, and fully-flexed knee.

TABLES CAPTIONS

Table 1. Number of nodes and elements of the three-dimensional (3D) models of the anthropoid patellae used in this work. Nature of the models refers to living (extant) or extinct (fossil) anthropoids, and patellar 3D models that have been digitally transformed in this study (modified). See 'Material and methods' for a further explanation on the modified patellae (NoApex, digitally removed apes; WApex, digitally added apex).

Patellar model	*Species*	*Catalogue no.*	*Nature*	*Nodes*	*Elements*
Cebus	*Cebus olivaceus*	AMNH42873	Extant	394,422	265,287
Ateles	*Ateles belzebuth*	AMNH259	Extant	331,604	221,888
Cercopithecus	*Cercopithecus mitis*	AMNH52402	Extant	270,139	181,383
Mandrillus	*Mandrillus sphinx*	AMNH89358	Extant	427,434	285,657
Colobus	*Colobus guereza*	AMNH52241	Extant	446,929	300,227
Hylobates	*Hylobates lar*	MCZ41412	Extant	403,089	268,374
Symphalangus	*Symphalangus syndactylus*	AMNH106581	Extant	439,722	295,965
Pongo	*Pongo pygmaeus*	AMNH62586	Extant	368,020	247,551
Pan	*Pan troglodytes*	MCZ23164	Extant	383,969	256,695
Gorilla	*Gorilla gorilla*	AMNH9029	Extant	363,359	246,392
Homo	*Homo sapiens*	SBU collection	Extant	356,758	240,169
Cercopithecus-NoApex	-	-	Modified	272,467	182,826
Gorilla-WApex	-	-	Modified	428,921	289,836
Pongo-WApex	-	-	Modified	327,870	218,663
Pierolapithecus	*Pierolapithecus catalaunicus*	IPS21350.37	Fossil	337,482	224,277

Table 2. Scaled forces (in N) of patellae 3D models. Scaled forces were based on patellae volume (mm^3) and calculated following equation (1) in the text to stress comparisons among patellar models in each of the three steps of knee flexion: extended knee (0º), semi-flexed knee (30º), and full-flexed knee (60º). Abbreviations: F, force; X, force applied in X direction; Y, force applied in Y direction.

			F extended knee		*F semi-flexed knee*		*F full-flexed knee*	
Patellar model	*Volume*	*Applied F*	*X*	*Y*	*X*	*Y*	*X*	*Y*
Cebus	312.44	0.599	0.599	0.000	0.519	0.299	0.299	0.519
Ateles	880.48	1.195	1.195	0.000	1.035	0.597	0.597	1.035
Cercopithecus	674.12	1.000	1.000	0.000	0.866	0.500	0.500	0.866
Mandrillus	1,019.80	1.318	1.318	0.000	1.141	0.659	0.659	1.141
Colobus	1,118.50	1.402	1.402	0.000	1.214	0.701	0.701	1.214
Hylobates	556.05	0.880	0.880	0.000	0.762	0.440	0.440	0.762
Symphalangus	1,258.80	1.516	1.516	0.000	1.313	0.758	0.758	1.313
Pongo	4,240.00	3.407	3.407	0.000	2.951	1.704	1.704	2.951
Pan	4,353.40	3.468	3.468	0.000	3.003	1.734	1.734	3.003
Gorilla	12,892.00	7.151	7.151	0.000	6.193	3.576	3.576	6.193
Homo	12,719.00	7.087	7.087	0.000	6.138	3.544	3.544	6.138
Cercopithecus-NoApex	623.70	0.949	0.949	0.000	0.822	0.475	0.475	0.822
Gorilla-WApex	14,590.00	7.766	7.766	0.000	6.726	3.883	3.883	6.726
Pongo-WApex	4,419.50	3.503	3.503	0.000	3.034	1.751	1.751	3.034
Pierolapithecus	2,405.10	2.335	2.335	0.000	2.022	1.167	1.167	2.022

Data from: Knee function through Finite Element Analysis and the role of Miocene hominoids to understand the origin of antipronograde behaviours: the *Pierolapithecus catalaunicus*' patella as a test-case study

MARTA PINA, DANIEL DeMIGUEL, FRANCESC PUIGVERT, JORDI MARCÉ-NOGUÉ and SALVADOR MOYÀ-SOLÀ

Appendix S1 Snapshots of computer-aided design (CAD) models of anthropoid patellae. Snapshots are shown in lateral (left; top, proximal, left, posterior) and posterior (right; top, proximal, left, lateral) views. A, *Cebus olivaceus*; B, *Cercopithecus mitis*; C, *Colobus guereza*; D, *Symphalangus syndactylus*; E, *Ateles belzebuth*; F, *Mandrillus sphinx*; G, *Hylobates lar*; H, *Homo sapiens*; I, *Pan troglodytes*; J, *Pongo pygmaeus*; K, *Gorilla gorilla*; L, *Pierolapithecus catalaunicus*; M, *Cercopithecus*-NoApex; N, *Gorilla*-WApex; O, *Pongo*-WApex. Scale bar = 10 mm.

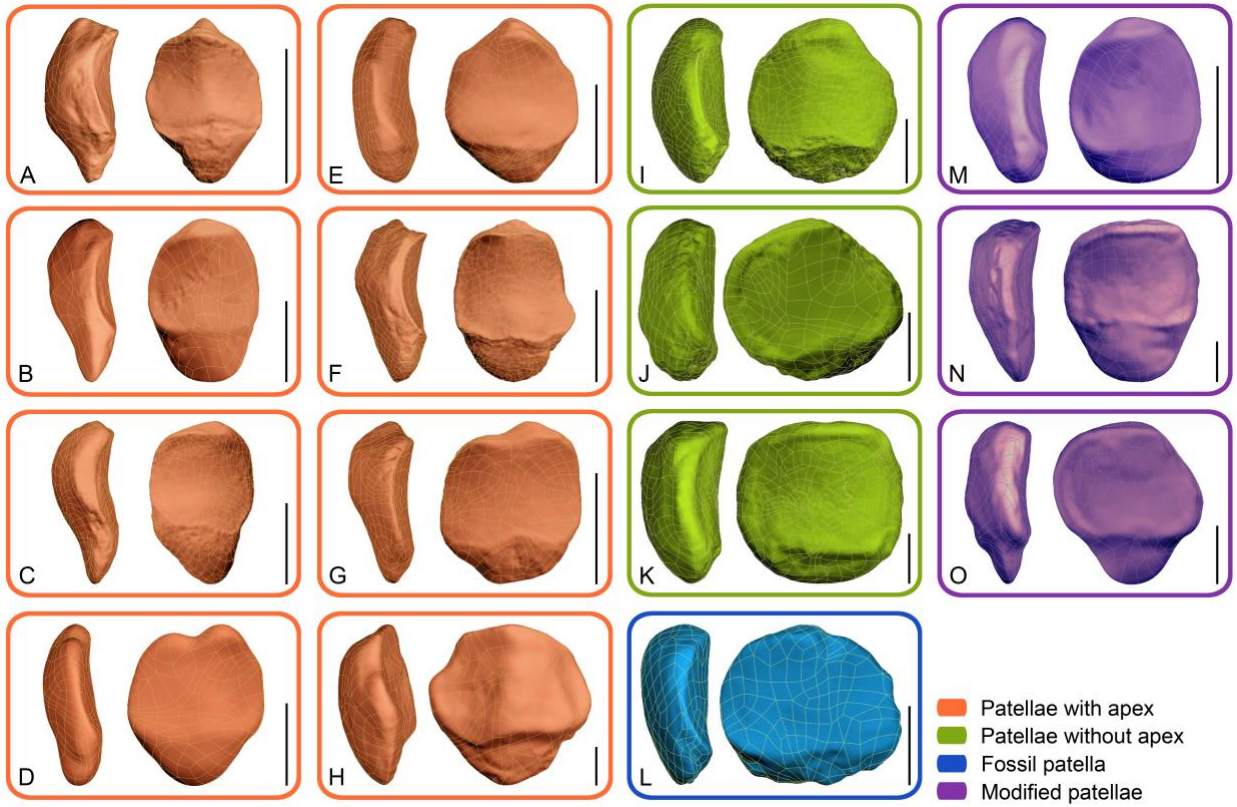

Appendix S2 Von Mises stress values (KPa) obtained at points A to E (Fig. 3) in every stage of knee flexion (0, extended; 30, semi-flexed; 60, fully-flexed).

	A			B			C			D			E		
	0	30	60	0	30	60	0	30	60	0	30	60	0	30	60
Cebus olivaceus	0.618	12.368	28.265	15.502	12.573	23.973	9.062	13.116	25.536	11.228	7.140	12.835	11.454	10.080	10.694
Ateles belzebuth	1.134	7.019	34.087	10.912	20.332	27.480	13.431	10.098	15.609	3.418	8.342	12.508	10.608	15.498	15.499
Cercopithecus mitis	0.617	10.859	24.673	4.615	18.004	22.984	14.850	7.629	14.150	1.899	4.994	8.567	5.626	12.972	9.668
Mandrillus sphinx	0.719	7.024	23.685	2.726	19.537	17.926	13.376	9.798	18.703	6.106	7.177	13.833	3.809	12.722	8.195
Colobus guereza	0.726	10.996	21.353	6.432	20.480	18.960	16.082	13.340	25.757	4.268	8.643	16.605	7.019	14.024	9.647
Hylobates lar	0.572	6.886	21.305	2.274	19.036	17.906	11.560	11.411	22.025	2.842	8.291	16.111	3.784	11.359	6.928
Symphalangus syndactylus	0.720	10.042	27.953	16.285	10.861	20.057	12.890	10.453	18.512	0.972	7.786	13.466	11.641	10.819	12.062
Pongo pygmaeus	0.790	7.917	22.012	9.247	19.454	14.890	17.582	9.998	20.370	15.340	10.471	21.255	8.759	14.408	8.507
Pan troglodytes	0.818	10.527	21.348	12.521	12.321	19.686	13.389	11.267	21.449	11.007	11.821	21.925	10.338	9.217	10.294
Gorilla gorilla	1.179	11.746	11.737	8.191	14.710	7.123	14.202	1.486	3.156	7.606	1.289	2.531	6.293	8.367	1.562
Homo sapiens	1.475	13.103	22.659	8.047	14.096	18.741	13.217	8.248	17.555	3.868	10.706	17.696	7.824	12.355	8.992
Pierolapithecus catalaunicus	1.018	6.880	24.995	7.131	17.466	17.823	12.496	9.179	20.099	8.894	8.991	19.835	7.201	11.430	6.677

Appendix S3

Validation test

In order to check if subtle differences on the patellar distal apex affects the final whole deformation of the virtually obtained geometries, a validation test is performed by slightly modifying different parameters of the apex. To do so, the *Gorilla*-WApex patella was selected. Its virtually added apex was modified again in terms of volume (increasing and decreasing a 15%), length (adding and subtracting 1/3 of its original length), inclination (adding 15º of inclination anteriorly and posteriorly), and shape (sharper and more rounded).

The eight new models were processed as the rest of geometries, following the same kinematic model explained in the main text. Von Mises stress colour maps and values were obtained (Appendices S4 and S5, respectively) for the eight models. Stress values were selected at points A-E (see main text and Appendix S5). Given that the objective of this additional test is checking if there are differences among these patellae, a Kruskal-Wallis non-parametric test was applied after testing for normality by the Shapiro-Wilk test (p-value < 0.05). Differences were checked at the three stages of knee flexion: extended (0), semi-flexed (30), and fully-flexed (60).

Von Mises stress colour maps show that there are scant differences among the models. Uniquely, the *Gorilla*-WApex model with a shorter apex displays some differences in stress distribution, mainly at the fully-flexed knee stage (Appendices S4D). Von Mises stress in this model is more widely spread along the third distal region of the bone, resembling the distribution observed in the patella of *Cebus* (Fig. 4A in the main text), whose apex is shorter than in *Cercopithecus* (Fig. 4C in the main text). This type of distribution also resembles that of great apes (except gorillas), which have patellae without distal apex (Fig. 4H, I in the main text). However, when stress values are

statistically analysed, no differences are found among the groups (0: p-value = 1, chi-squared = 0.816; 30: p-value = 1, chi-squared = 0.438; 60: p-value = 1, chi-squared = 0.705).

Therefore, given that we do not find differences among the eight modified models, we can conclude that the original modified geometries are reliable representatives of a sample of patellae with different types of form variability at the distal apex (volume, length, inclination, and shape). This validation test allows us to also corroborate that a unique specimen accurately represent a group when working with FEA.

Appendix S4 Von Mises stress distribution (in MPa) in the mid-sagittal section (top, superior; left, posterior) of the modified patellar models derived from that originally modified *Gorilla*-WApex (*Gorilla* with a virtually added distal apex). These models show subtle modifications of the *Gorilla*-WApex distal apex in terms of volume (**A**, **B**), length (**C**, **D**), inclination (**E**, **F**), and shape (**G**, **H**), and are represented in three knee stages: extended (left), semi-flexed (middle), and full-flexed (right) joint. **A**, 15% larger apex; **B**, 15% smaller apex; **C**, 1/3 longer apex; **D**, 1/3 shorter apex; **E**, 15º more anteriorly tilted apex; **F**, 15º more posteriorly tilted apex; **G**, sharper apex; and **H**, more rounded apex. Results homogenized according to the same stress scale (minimum = 0 MPa; maximum = 0.026 MPa).

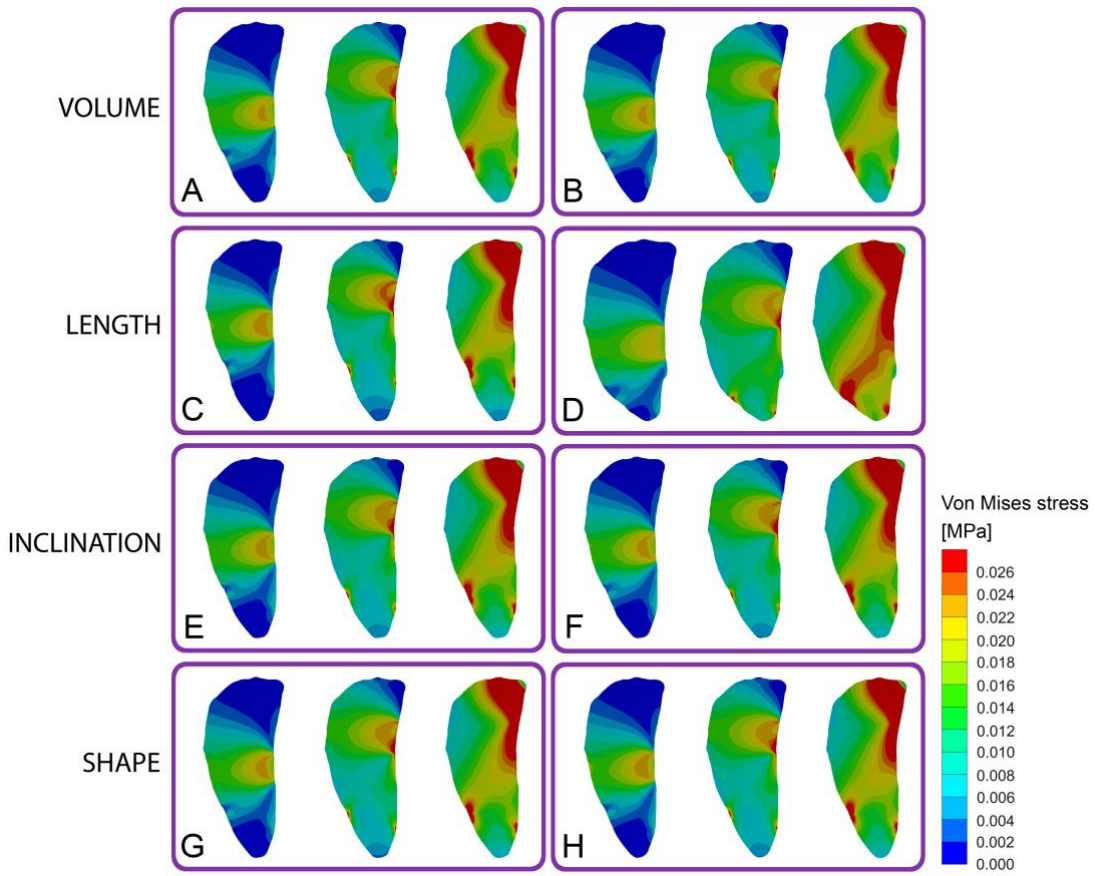

Appendix S5 Number of nodes and elements, volume (mm^3), and applied forces (F; in N) of the three-dimensional (3D) models derived from the virtually modified patella *Gorilla*-WApex. Scaled forces were based on patellae volume and calculated following equation (1) in the main text. Additionally, von Mises stress values (KPa) obtained at points A to E (Fig. 3 in the main text) in every stage of knee flexion (0, extended; 30, semi-flexed; 60, fully-flexed). Then name of the model refers to the modification applied to the *Gorilla*-WApex new apex (see Appendix S3 for further explanation).

					0					*30*					*60*				
	Nodes	Elements	Volume	Applied F	A	B	C	D	E	A	B	C	D	E	A	B	C	D	E
Bigger	430238	287456	14495	0.679	1.031	3.833	5.834	1.551	6.885	0.015	23.386	10.532	7.896	15.209	23.937	20.337	16.964	13.321	9.030
Smaller	462939	311744	14179	0.717	1.026	3.916	5.625	1.639	6.970	0.015	22.980	10.931	8.354	15.018	23.565	20.064	17.410	14.120	8.904
Longer	470893	316042	15056	0.724	1.068	4.056	6.114	1.295	7.203	0.015	23.927	10.333	7.507	15.584	24.555	20.870	16.732	12.697	9.259
Shorter	380813	252028	13375	0.622	1.002	3.807	5.686	2.264	6.714	0.014	22.243	12.978	11.249	14.538	22.849	19.977	21.140	18.398	9.099
Anterior	513540	344049	14561	0.766	1.027	3.930	5.929	1.476	7.023	0.015	23.491	10.458	7.871	15.223	24.153	20.564	16.874	13.274	9.051
Posterior	427772	285636	14577	0.676	1.030	4.122	6.247	1.441	7.037	0.015	23.298	10.316	7.675	15.110	23.750	20.082	16.828	13.032	8.928
Sharper	441951	296609	14493	0.694	1.039	3.968	5.910	1.486	7.030	0.015	23.330	10.371	7.858	15.193	23.924	20.286	16.763	13.245	8.991
Rounded	480277	323909	14701	0.735	1.017	4.017	6.113	1.432	7.229	0.015	23.427	10.328	7.903	15.234	24.018	20.557	16.746	13.333	9.101

Appendix S6 Principal Component Analysis (PCA) results. ANOVA and MANOVA p-value results for the points (A-E) selected at the midsagittal slice of the patellar sample. Comparisons were performed for three group categories: Ap, presence *vs* absence of patellar apex; BP, pronograde *vs* orthograde primates; and BPAp (Ap + BP), pronograde primates with apex, orthograde primates with apex, and orthograde primates without apex. Analyses were made at every stage of knee flexion (0, extended; 30, semi-flexed; 60, fully-flexed). *, $p < 0.05$; NS, $p > 0.05$ (not significant).

	Ap			BP			BPAp		
ANOVA	*0*	*30*	*60*	*0*	*30*	*60*	*0*	*30*	*60*
A	NS	NS	NS	NS	NS	NS	NS	NS	NS
B	NS	NS	*	NS	NS	NS	NS	NS	NS
C	NS	NS	NS	NS	NS	NS	NS	NS	NS
D	*	NS	NS	NS	NS	NS	*	NS	NS
E	NS	NS	NS	NS	NS	NS	NS	NS	NS
MANOVA	NS	NS	NS	NS	NS	NS	NS	NS	NS

Appendix S7 Principal Component Analysis (PCA) loadings for the variables (points A to E) analyzed in this study in the first two principal components (PC). PCA were repeated in every stage of knee flexion (0, extended; 30, semi-flexed; 60, fully-flexed).

	PC1	PC2
A0	-0.003	0.004
B0	-0.768	0.364
C0	0.081	-0.179
D0	-0.439	-0.890
E0	-0.459	0.209
A30	0.366	-0.166
B30	-0.649	0.519
C30	-0.416	-0.611
D30	-0.321	-0.566
E30	-0.410	0.095
A60	-0.484	-0.455
B60	-0.466	-0.404
C60	-0.548	0.438
D60	-0.392	0.618
E60	-0.307	-0.239

Appendix S8 Principal Component Analysis (PCA) eigenvalues of every taxon for the first two principal components (PC). PCA were repeated in every stage of knee flexion (0, extended; 30, semi-flexed; 60, fully-flexed).

	0		30		60	
	PC1	PC2	PC1	PC2	PC1	PC2
Cebus olivaceus	-1.668	4.112	-5.148	2.247	-8.477	-12.408
Ateles belzebuth	-9.360	-0.207	3.197	-4.346	-8.122	-2.649
Cercopithecus mitis	6.239	1.871	0.908	3.567	2.310	-7.989
Mandrillus sphinx	6.560	-2.675	-2.993	2.412	1.038	0.100
Colobus guereza	3.263	0.497	-4.630	-0.628	-3.714	5.194
Hylobates lar	8.205	0.383	-3.189	0.429	-0.126	4.354
Symphalangus syndactylus	-5.239	8.557	4.055	-3.516	-2.960	-3.935
Pongo pygmaeus	-4.435	-8.232	-4.445	0.395	-0.654	7.326
Pan troglodytes	-6.112	-2.104	2.307	-5.773	-3.969	6.149
Gorilla gorilla	0.628	-1.645	9.008	7.126	26.846	-2.299
Homo sapiens	1.596	2.125	2.427	-2.504	0.027	1.930
Pierolapithecus catalaunicus	0.324	-2.683	-1.496	0.590	-2.199	4.226